



1 Scenario set-up and the new CMIP6-based climate-related forcings provided within the
2 third round of the Inter-Sectoral Model Intercomparison Project (ISIMIP3b, group I and II)

3

4 Katja Frieler^{1,2}, Stefan Lange¹, Jacob Schewe¹, Matthias Mengel¹, Simon Treu^{1,2}, Christian Otto¹, Jan
5 Volkholz¹, Christopher P.O. Reyer¹, Stefanie Heinicke¹, Colin Jones³, Julia L. Blanchard⁴, Cheryl S.
6 Harrison⁵, Colleen M. Petrik⁶, Tyler D. Eddy⁷, Kelly Ortega-Cisneros⁸, Camilla Novaglio⁴, Ryan Heneghan⁹,
7 Derek P. Tittensor¹⁰, Olivier Maury¹¹, Matthias Büchner¹, Thomas Vogt¹, Dánnell Quesada Chacón¹, Kerry
8 Emanuel¹², Chia-Ying Lee¹³, Suzana J. Camargo^{13,14}, Jonas Jägermeyr^{14,15,1}, Sam Rabin^{16,a,b}, Jochen Klar¹,
9 Iliusi D. Vega del Valle¹, Lisa Novak¹, Inga J. Sauer¹, Gitta Lasslop¹⁷, Sarah Chadburn¹⁸, Eleanor Burke¹⁹,
10 Angela Gallego-Sala²⁰, Noah Smith²¹, Jinfeng Chang²², Stijn Hantson²³, Chantelle Burton¹⁹, Anne Gädeke¹,
11 Fang Li²⁴, Simon N Gosling²⁵, Hannes Müller Schmied^{17,26}, Fred Hattermann¹, Thomas Hickler¹⁷, Rafael
12 Marcé²⁷, Don Pierson²⁸, Wim Thiery²⁹, Daniel Mercado-Bettín²⁷, Robert Ladwig³⁰, Ana I. Ayala²⁸, Matthew
13 Forrest¹⁷, Michel Bechtold³¹, Robert Reinecke³², Inge de Graaf³³, Jed O. Kaplan³⁴, Alexander Koch³⁵,
14 Matthieu Lengaigne¹¹

15

16 Affiliations:

17 ¹Potsdam Institute for Climate Impact Research, 14473 Potsdam, Germany

18 ²University of Potsdam, Institute for Environmental Science and Geography, 14476 Potsdam, Germany

19 ³National Centre for Atmospheric Science and School of Earth and Environment, University of Leeds,
20 Leeds, LS29JT, UK

21 ⁴Institute for Marine and Antarctic Studies, University of Tasmania, Hobart, Tasmania, Australia

22 ⁵Department of Ocean and Coastal Science and Center for Computation and Technology, Louisiana State
23 University, Baton Rouge, Louisiana, USA

24 ⁶Scripps Institution of Oceanography, University of California San Diego, CA, USA

25 ⁷Centre for Fisheries Ecosystems Research, Fisheries & Marine Institute, Memorial University, St. John's,
26 NL, Canada

27 ⁸Marine and Antarctic Research for Innovation and Sustainability, Department of Biological Sciences,
28 University of Cape Town, Rondebosch, Cape Town, 7701, South Africa

29 ⁹School of Environment and Science, Griffith University, Brisbane, Queensland, Australia

30 ¹⁰Department of Biology, Dalhousie University, Halifax, Nova Scotia, Canada, B3H 4R2

31 ¹¹IRD, Univ Montpellier, CNRS, Ifremer, INRAE, MARBEC, Sète, France

32 ¹²Lorenz Center, Massachusetts Institute of Technology, Cambridge, MA, USA

33 ¹³Lamont-Doherty Earth Observatory, Columbia University, Palisades, New York, USA

34 ¹⁴Columbia Climate School, Columbia University, New York, NY 10025, USA

35 ¹⁵NASA Goddard Institute for Space Studies, New York, NY 10025, USA

36 ¹⁶Climate and Global Dynamics Laboratory, National Center for Atmospheric Research Boulder, CO
37 80302, USA

38 ¹⁷Senckenberg Leibniz Biodiversity and Climate Research Centre (SBiK-F), Frankfurt am Main, Germany.

39 ¹⁸Department of Mathematics, University of Exeter, Exeter UK

40 ¹⁹Met Office Hadley Centre, Fitzroy Road, Exeter, UK

41 ²⁰Geography Department, University of Exeter, Exeter, UK



- ²¹College of Engineering, Mathematics and Physical Sciences, University of Exeter, Exeter EX4 4QF, UK.
- ²²College of Environmental and Resource Sciences, Zhejiang University, Hangzhou, China
- ²³Faculty of Natural Sciences, Universidad del Rosario, Bogotá, Colombia
- ²⁴International Center for Climate and Environment Sciences, Institute of Atmospheric Physics, Chinese Academy of Sciences, Beijing, China
- ²⁵School of Geography, University of Nottingham, Nottingham, UK
- ²⁶Institute of Physical Geography, Goethe University Frankfurt, Frankfurt am Main, Germany
- ²⁷Blanes Centre for Advanced Studies (CEAB-CSIC), Blanes, Spain
- ²⁸Department of Ecology and Genetics, Uppsala University, Norbyvägen 18 D, 752 36 Uppsala, Sweden
- ²⁹Vrije Universiteit Brussel, Department of Water and Climate, Brussels, Belgium
- ³⁰Department of Ecoscience, Aarhus University, C.F. Møllers Allé 3, 8000 Aarhus C, Denmark
- ³¹KU Leuven, Department of Earth and Environmental Sciences, Leuven, Belgium
- ³²Johannes Gutenberg-University Mainz, Mainz, Germany
- ³³Earth Systems and Global Change Group, Wageningen University and Research, Wageningen, The Netherlands
- ³⁴Department of Earth Sciences and Institute for Climate and Carbon Neutrality, The University of Hong Kong, Hong Kong
- ³⁵Simon Fraser University, Burnaby, British Columbia, CA
- ^aformerly at: Institute of Meteorology and Climate Research / Atmospheric Environmental Research, Karlsruhe Institute of Technology, Garmisch-Partenkirchen, Germany
- ^bformerly at: Department of Environmental Sciences, Rutgers University, New Brunswick, New Jersey, USA

64

65 Correspondence to: Katja Frieler (katja.frieler@pik-potsdam.de)

66

Abstract. This paper describes the climate-related forcings (CRFs) provided within the ‘b’ part of the third simulation round of the Inter-Sectoral Impact Model Intercomparison Project (ISIMIP3b). While ISIMIP3a comprises historical impact models simulations forced by observational CRF and direct human forcings (DHF), the ISIMIP3b CRFs are based on climate model simulations generated within the sixth phase of the Coupled Model Intercomparison Project (CMIP6). In a first set of experiments (ISIMIP3b, group I) the CMIP6-based CRFs for the historical period are combined with historical observation-based DHF also considered in ISIMIP3a (e.g. land use patterns, water and agricultural management, and fishing efforts). These group I simulations allow for the quantification of impacts of historical climate change by comparison to simulations where the observational DHF are combined with simulated pre-industrial CRFs. In addition, the impacts of observed changes in CRFs can be compared to the impacts of simulated changes in CRFs by comparing the ISIMIP3a simulations to the ISIMIP3b, group I simulations. The second group of experiments (ISIMIP3b, group II) comprises future projections assuming constant observational direct human forcings at 2015 levels to estimate the impact of climate change given today’s direct human influences for the low emission scenario SSP1-2.6, the high and the very high emission scenarios SSP3-7.0, SSP5-8.5, respectively. The very high emissions scenarios and the assumption of fixed present day direct human forcings particularly allow for testing the scalability of impacts in terms of global temperature change. The provided CRFs comprise atmospheric CO₂ and CH₄ concentrations,



84 atmospheric and oceanic climate data, coastal water levels, tropical cyclone tracks and their associated
85 wind speed and precipitation fields. In addition to the CRFs data, this paper describes the experiments
86 belonging to group I and II and the rationale behind them. Another set of future projections accounting
87 for changing DHFs (ISIMIP3b, group III) is in preparation and will be described in another paper.

88

89

90 Introduction

91 This is the second paper of a series of three papers describing the experiments of the third simulation
92 round of the Inter-Sectoral Impact Model Intercomparison Project ISIMIP (isimip.org). The project
93 provides a common scenario framework for cross-sectorally consistent climate impact simulations. In its
94 third round it covers i) model evaluation and climate impact attribution experiments based on
95 observation-based climate and direct human forcings (ISIMIP3a, first paper, (Frieler et al., 2023)), ii)
96 climate impact simulations driven by simulated climate-related forcings based the sixth phase of the
97 Coupled Climate Model Intercomparison Project (CMIP6) assuming ISIMIP3a observational DHF in the
98 historical period and fixed 2015 DHF for the future simulations (ISIMIP3, group I+II, this paper), and iii)
99 an upcoming set of CMIP6-based future projections where DHF vary according to given Shared
100 Socioeconomic Pathways (SSPs) (no adaptation scenarios) and in response to climate change impacts
101 (adaptation scenarios) (ISIMIP3b, group III). So while this paper only describes the ISIMIP3b
102 climate-related forcings, the third paper will only address the DHFs that are still under development
103 while the CRF of the group III simulations will be identical to the future CRF described here.

104

105 Similar to the Coupled Model Intercomparison Project (CMIP) (Eyring et al., 2016) all simulations will be
106 freely available (<https://data.isimip.org/>) to allow for follow-up analysis. The consistent design of the
107 simulations does not only allow for the comparison of climate impact simulations within each sector,
108 but also enables the bottom-up integration of impacts across sectors. Thus, it provides a unique basis
109 for the estimation of the effects of climate change on, e.g., the economy, displacement and migration,
110 health, or water quality resolving the mechanisms along different impact channels and fully exploiting
111 the process-understanding represented in the biophysical impact models.

112

113 Compared to ISIMIP2b, the ISIMIP3b CRF represent the following updates: i) climate forcing data based
114 on phase 6 of the Coupled Model Intercomparison Project (CMIP6) (Eyring et al., 2016) and
115 post-processed by an improved bias adjustment and statistical downscaling method (see section 3.2),
116 and ii) large ensembles of potential realisations of tropical cyclone tracks, wind and precipitation fields
117 derived from two different modelling approaches assuming CMIP6 boundary conditions, while in
118 ISIMIP2b only one approach was used and precipitation fields were not included. In addition, we plan to
119 provide coastal water levels at high temporal resolution (upcoming). The approach to generate the data
120 is also described here.

121

122 The development of the ISIMIP3b protocol was coordinated by the ISIMIP-Cross-Sectoral Science Team
123 (CSST) at the Potsdam Institute for Climate Impact Research (PIK) along the same decision process as for
124 ISIMIP3a (Frieler, submitted 2023).

125



126 This paper is accompanied by a simulation protocol (*ISIMIP3b Simulation Protocol*, 2023) providing all
127 technical details such as file and variable naming conventions, as well as sector-specific output variables
128 to be reported by the participating modelling teams. This paper refers to the protocol version of
129 December 21st, 2023. However, as the protocol may still be updated due to addition of new variables,
130 correction of errors, or the inclusion of new sectors, contributors to ISIMIP should always refer to
131 protocol.isimip.org for the most up to date reference for planned impact model simulations.

132

133 The ISIMIP3a and ISIMIP3b protocols have been jointly developed and participation in ISIMIP3 requires
134 contribution to both ISIMIP3a and ISIMIP3b, using the same impact model versions in order to allow for
135 the evaluation of the impact models future projections in ISIMIP3b.

136

137 In the following, we describe the rationale behind the individual scenario set-ups (section 1). We then
138 introduce the individual climate-related forcing data sets in the second section covering atmospheric
139 climate data including lightning and tropical cyclones tracks, wind and precipitation fields; ocean data;
140 coastal water levels; and atmospheric CO₂ as well as CH₄ concentrations.

141

142 **1 Experiments and underlying rationale**

143

144 The selection of ISIMIP3b scenarios (see **Figure 1**) was generally motivated by the aim to i) capture a
145 wide range of possible futures from low to high emission scenarios, ii) the availability of climate model
146 simulations, and iii) the provision of a long baseline simulation assuming pre-industrial climate
147 conditions that allows for a robust estimation of reference return levels of extreme events. Given recent
148 mitigation efforts, some estimates of recoverable coal reserves, and decreasing prices for renewable
149 energies the emissions underlying SSP5-8.5 have been criticised for not representing a meaningful
150 ‘business as usual scenario’ (Hausfather & Peters, 2020). Therefore, within ISIMIP SSP5-8.5 is not
151 considered a ‘business as usual scenario’, but rather a worst case scenario. Furthermore, its strong
152 warming signal allows testing to what degree the simulated impacts of climate may scale with global
153 mean temperature, which could potentially lead to translating impacts to other emission scenarios. In
154 addition, even under lower emission scenarios, global warming levels as the ones reached under
155 SSP5-8.5 in 2100 will only be reached later in time as long as emissions are not reduced to zero. These
156 impacts of high warming levels would not be captured when only considering lower emission scenarios
157 ending in 2100. In response to the discussion, the ‘average no climate protection policy’ SSP3-7.0
158 (Hausfather & Peters, 2020) has been added to the ISIMIP3b protocol. However, SSP3-7.0 has not been
159 designed as a business as usual scenario, either. Instead it is based on rather extreme assumptions
160 about land use changes and aerosol emissions e.g. leading to a scaling of precipitation with global mean
161 temperature that diverges from the scaling identified in the other scenarios (Shiogama et al., 2023).

162

163 All ISIMIP experiments are determined by the underlying set of CRFs and DHF, where each package of
164 CRF and DHF has a specific label that will then be included in the output file names to allow for an
165 identification of the experiments they belong to. The individual experiments are defined by the
166 combination of both types of forcing data sets, where the associated specifiers are indicated in brackets
167 in the subheadings naming the experiments (CRF specifier + DHF specifier). The different combinations



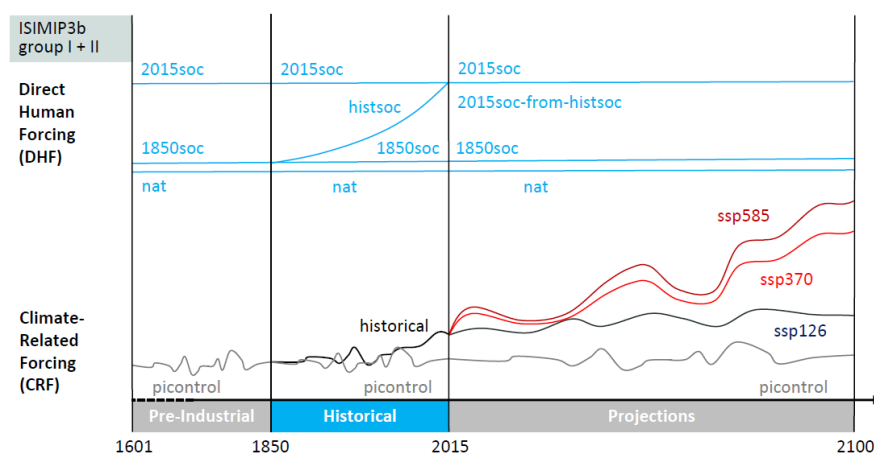
of the default sets of ISIMIP3b CRFs ('picontrol', 'historical', 'ssp126', 'ssp370', and 'ssp585') and DHF ('histsoc', '2015soc', '1901soc', '1850soc', 'nat', and '2015soc-from-histsoc') are sketched in **Figure 1** and described in more detail below.

171

The CRF forcing data described in this paper are mandatory; i.e. if impact models consider this forcing, the specified dataset must be used; if an alternative input data set is used instead, the run cannot be considered an ISIMIP3, group I + II simulation. The DHF for the historical period is identical to the ISIMIP3a DHF listed in **Table 1** of (Frieler, submitted 2023) where we also indicate whether the data set is mandatory or optional. Optional forcing data could be used but is not mandatory. In addition, the protocol includes a set of sensitivity experiments that are described as deviations from the default runs and labelled by the baseline CRF and DHF settings and a third specifier indicating the deviation from this default setting. The ISIMIP3b group I+II sensitivity runs include experiments with fixed levels of atmospheric CO₂ concentrations ('2015co2'), high levels in CO₂ concentrations in combination with low levels of climate change ('ssp585co2'), and runs with lightning data that vary in response to climate change ('varlightning'), while lightning is fixed at present day levels in the default runs. These sensitivity experiment runs are not depicted in Figure 1 but listed in **Table 2**.

184

185



186

Figure 1: Illustration of the default ISIMIP3b forcing data sets. Each ISIMIP3b experiment is defined by a combination of a CRF data set with a DHF data set. The considered combinations are listed in **Table 2** and the underlying rationale is described in section 1.1 and 1.2. **Table 1** lists all data sets defining the considered CRFs while the DHFs are based on the same datasets as in ISIMIP3a. Potentially required spin-up procedures are not included in the Figure, but described in section 1.1.

192

The ISIMIP3b simulations are divided into two groups. Group I comprises the simulations from 1601 - 1849 (pre-industrial) and 1850 - 2014 (historical) assuming simulated pre-industrial and historical CRFs and different constant ('nat', '1850soc', and '2015soc') or varying ('histsoc') levels of DHF based on the



196 same observational data used in ISIMIP3a (see **Figure 1**). Group II comprises the future projections
197 assuming constant 2015 levels of DHF (see **Figure 1**) including a baseline with pre-industrial CRF (grey
198 line in the future projections part of **Figure 1**). All experiments are introduced in more detail below
199 (section **1.1** for group I and **1.2** for group II).

200

201 In contrast to ISIMIP3a, the CRFs provided for ISIMIP3b currently only comprise atmospheric (see
202 section **2.1**) and oceanic climate data (see section **2.4**), tropical cyclone tracks with associated wind and
203 precipitation fields (see section **2.2**), and CO₂ and methane concentration (see section **2.5**). We do not
204 yet provide associated coastal water levels (see section **2.2.3** for planned work), and lightning data (see
205 **Table 5**). Impact simulations that rely on the missing forcings cannot be generated within ISIMIP3b yet,
206 but we are currently developing their setup and will provide the forcings as soon as possible. The
207 ISIMIP3b atmospheric and oceanic climate data is derived from five different General Circulation Models
208 generated within the Coupled Model Intercomparison project, phase 6 (CMIP6).

209

210 **Table 1: Climate-Related Forcing datasets for ISIMIP3b.**

Forcing	Status	Source, description
Climate-related forcings ('picontrol', 'historical', 'ssp126', 'ssp370', 'ssp585')		
Atmospheric forcings ('picontrol', 'historical', 'ssp585', 'ssp370', 'ssp126')		
Gridded atmospheric climate forcing	mandatory	Bias-adjusted data (pre-industrial climate, historical climate, and future projections for the SSP1-2.6, SSP3-7.0, and SSP5-8.5 scenarios) generated by GFDL-ESM4, IPSL-CM6A-LR, MPI-ESM1-2-HR, MRI-ESM2-0, and UKESM1-0-LL within CMIP6, see section 2.1
Local atmospheric climate forcing for lakes	mandatory	Atmospheric data extracted from the data sets above for 72 lakes that have been identified within the lake sector as locations (grid cell of the ISIMIP 0.5° grid, ISIMIP3 local lake sites) where models can be calibrated based on observed temperature profiles and hypsometry within ISIMIP3b (depth and area).
Tropical cyclone tracks with wind and precipitation fields	mandatory	Available on request (see section 2.2), samples of synthetic tropical cyclone tracks derived from the five CMIP6 GCMs considered within ISIMIP generated by two different statistical downscaling approaches, see section 2.2 . MIT approach (Emanuel et al., 2008): historical climate from IPSL-CM6A-LR, MPI-ESM1-2-HR, UKESM1-0-LL and GFDL-ESM4 (all 1850-2014), and from MRI-ESM2-0 (1950-2014). Future climate: ssp370 and ssp585 (2015-2100) from IPSL-CM6A-LR, MPI-ESM1-2-HR, MRI-ESM2-0, UKESM1-0-LL, and ssp585 (2061-2100) from GFDL-ESM4.



		Two different configurations (SD and CRH, see section 2.2) of the Columbia HAZard model (CHAZ, (Lee et al., 2018)): pre-industrial climate (1601-2100) from GFDL-ESM4, IPSL-CM6A-LR, MPI-ESM1-2-HR, MRI-ESM2-0, and UKESM1-0-LL. historical climate (1850-2014) from GFDL-ESM4, IPSL-CM6A-LR, MPI-ESM1-2-HR, MRI-ESM2-0, and UKESM1-0-LL future climate (2015-2100): ssp126, ssp370, ssp585 from GFDL-ESM4, IPSL-CM6A-LR, MPI-ESM1-2-HR, MRI-ESM2-0, and UKESM1-0-LL
Lightning	mandatory	Flash Rate Monthly Climatology from (Cecil, 2006), not changing with climate change
Oceanic forcings ('picontrol', 'historical', 'ssp585', 'ssp370', 'ssp126')		
Oceanic climate forcing	mandatory	Uncorrected data (pre-industrial climate, historical climate, and future projections for the SSP1-2.6, SSP3-7.0, and SSP5-8.5 scenarios) generated by GFDL-ESM4, IPSL-CM6A-LR, MPI-ESM1-2-HR, and UKESM1-0-LL within CMIP6, see section 2.4
Coastal water levels		
Coastal water levels	mandatory	Not available yet, but we plan to provide hourly water levels derived from the atmospheric forcings described above combined with long-term sea-level trends; see section 2.3 .
Atmospheric composition or fluxes		
Atmospheric CO ₂ concentration	mandatory	(Büchner & Reyer, 2022) based on the following sources: 1850-2005: (Meinshausen et al., 2011); 2006-2014: Global annual CO ₂ from NOAA Global Monthly Mean CO ₂ ((Lan et al., 2023); 2015-2100: (Meinshausen et al., 2020)
Atmospheric CH ₄ concentration	mandatory	(Büchner & Reyer, 2022) based on the following sources: 1850-2014: (Meinshausen et al., 2017); 2015-2100: (Meinshausen et al., 2020)
Climate-Related Forcings for the sensitivity experiment 'varlightning', using above forcing data except for:		
Lightning data ('varlightning')		
Varying lightning according to climate change	mandatory	Lightning data has been generated for the ssp126, ssp370, and ssp850 climate projections from UKESM1-0-LL (Kaplan et al., 2023)
Climate-Related Forcings for the 'de-biased' sensitivity experiment		
Global oceanic forcings		



Oceanic forcings based on de-biased atmospheric forcings	mandatory	Not available yet, simulated by the ocean biogeochemistry model ocean-biogeochemistry NEMO-PISCES forced by a de-biased version of the IPSL-CM6A-LR-based atmospheric forcing (see section 2.4.2)
Regional oceanic forcings		
De-biased oceanic forcing based on observed oceanic data for individual variables and regions	mandatory	Not centrally provided, see section 2.4.3

211

212

213 **1.1 ISIMIP3b, group I: Climate-model based impact model simulations for the period** 214 **from 1601 to 2015**

215

216 The group I experiments cover the years 1601-1849 with pre-industrial CRFs ('picontrol') and fixed 1850
217 direct human forcings ('1850soc') described in the grey column 3 of the ISIMIP3b scenario **Table 2** as
218 well as the subsequent years 1850-2014 considering pre-industrial and historical climate-related forcings
219 ('picontrol' or 'historical') and different assumptions about direct human forcings ('histsoc', '2015soc',
220 '1850soc', and 'nat') as described in the grey column 4 of **Table 2**. The reasoning behind the individual
221 experiments are introduced below.

222

223 **Pre-industrial reference simulations (picontrol + histsoc, picontrol + 2015soc, picontrol +**
224 **2015soc-from-histsoc, picontrol + 1850soc, picontrol + nat; default):** To estimate the impacts of
225 historical and future changes in the CRFs, the protocol includes reference simulations based on
226 pre-industrial CRFs and DHF identical to those considered in the climate change scenario runs. In order
227 to allow for the fitting of extreme value distributions, e.g. to estimate reference 100 year return levels of
228 certain impacts, the runs are designed to includes the generation of large samples (at least 250 years)
229 of impact distributions distribution based on stable pre-industrial CRFs (picontrol) and constant DHFs
230 (see 'picontrol + 1850soc', 'picontrol + 2015soc', and 'picontrol + nat' experiments in **Table 2**).

231 In addition, the protocol includes a reference experiment for the historical period (1850-2014) with DHF
232 changing over time (histsoc) and 1850-2014 pre-industrial CRF (picontrol), while fixed 2015 DHF is
233 considered afterwards (2015-2100) ('picontrol + 2015soc-from-histsoc'). This run may be different from
234 the 'picontrol + 2015soc' simulation for this time window because of the lagged effects of increasing
235 DHF from 1850 to 2014. The 'histsoc' DHF is identical to ISIMIP3a (Frieler, submitted 2023).

236 The complete pre-industrial reference runs are divided in two parts. Only the first parts from the start
237 until 2014 belong to group I (grey fields in the table), while the second parts covering the period
238 2015-2100 belong to group II (red parts of the table).

239

240 Comparing these reference simulations to the scenario experiments using historical CRFs (historical +
241 histsoc, historical + 2015soc, historical + 1850soc, historical + nat; default (see below)) allows for the



estimation of the effects of simulated historical climate change conditional on the assumed DHF. The historical climate-related forcing ('historical') starts from the pre-industrial climate simulation in 1850, i.e. the 'picontrol' and 'historical' versions of the experiments have a common starting point. As some impact indicators may have 'internal' trends not necessarily forced by external drivers (e.g. re-growth of forests), the comparison of the 1850-2014 impact simulations forced by the 'historical' CRF to parallel simulations using the 'picontrol' CRF is more appropriate to estimate the effects of historical climate change than comparing an early period of the historical impact simulation to the end of the historical period.

For models requiring a spin-up, the 'picontrol' CRFs should be used in combinations with DHF i) at 1850 levels to spin-up for the '1850soc' and 'histsoc' experiments, ii) at 2015 levels to initialise the '2015soc' experiment, and iii) set to zero to start the 'nat' experiments. For the spin-up the 'picontrol' CRF should be copied as often as needed. The 'picontrol + 1850soc' run from 1601-1849 is part of the regular experiments that should be reported and hence the spin-up has to be finished before this pre-industrial period.

To allow for a quantification of the impacts of the anthropogenic CRFs, we also support historical reference simulation assuming only natural CRF ('hist-nat' simulations generated within the Detection and Attribution Model Intercomparison Project (DAMIP) as sub-MIP of CMIP6, (Gillett et al., 2016) by providing the associated bias-adjusted CRF as secondary climate input data (Lange et al., 2023). However, associated simulations are not an official part of ISIMIP3b and not described in the associated protocol.

262

Standard historical simulations based on historical climate-related forcing and observed changes in direct human forcing (historical + histsoc; default): The historical simulations (1850-2014) are forced by historical ('historical') CRFs and DHFs evolving according to observations (ISIMIP3a 'histsoc' DHF). The ISIMIP3b 'historical + histsoc' experiment is comparable to the default 'obsclim + histsoc' run used in ISIMIP3a but based on simulated CRFs. The simulated climate is different from the observed realisation due to differences in the internal variability of the observed and simulated historical climate and potential deficits in the climate model simulations. A comparison between the default ISIMIP3b 'historical + histsoc' impact model simulations to the associated ISIMIP3a results allows for a quantification of the effects of the discrepancies between the observed and simulated CRFs on the considered impact indicators. This experiment can be initialised from the spin-up of the associated pre-industrial reference simulation in case a spin-up is needed.

274

Simulations with historical climate-related forcing and fixed 2015 direct human forcing (historical + 2015soc; default): This historical experiment is similar to the standard historical experiment except that it is forced by fixed 2015 DHF. It is introduced into the 'first priority' scenario-set-up to generate an ensemble of historical cross-sectorally consistent impact simulations that is as large as possible by not excluding impact models that are not able to handle varying DHF. If a spin-up is needed the experiment can be initialised from the spin-up of the associated pre-industrial reference simulation (picontrol + 2015soc, default) described at the beginning of this section.

282



283 Simulations with historical climate-related forcing and fixed 1850 direct human forcing (historical +
284 1850soc; default): This historical experiment is also similar to the standard historical experiment but it is
285 forced by the fixed 1850 DHFs. It corresponds to the ‘obsclim + 1901soc’ simulation of ISIMIP3a. Here in
286 ISIMIP3b we consider the year 1850 instead of 1901 used in ISIMIP3a as this is the year where the
287 ‘historical’ climate simulations with observed natural and human forcings start, i.e. a branch from the
288 pre-industrial climate simulations assuming constant pre-industrial forcings (‘picontrol’). If a spin-up is
289 required it does not have to be newly generated as it is identical to the spin-up for the default ‘picontrol
290 + 1850soc’, ‘picontrol + histsoc’, and ‘historical + histsoc’ experiments and described in the beginning of
291 this section.

292

293 Simulations with historical climate-related forcing and no direct human forcings (historical + nat;
294 default): Considering no direct human forcings (nature run) allows quantifying the effect of the
295 simulated historical climate change conditional on otherwise natural conditions, i.e. no direct human
296 influences on land use, water management etc.. This experiment is introduced as a companion
297 experiment to the ‘obsclim + nat’ simulations of ISIMIP3a. The comparison with the three historical
298 simulations with constant direct human forcings allows testing, to what degree the impact of climate
299 change on the simulated natural or human systems is conditional on the underlying direct human
300 forcing. This experiment is only included for the biomes and fisheries and marine ecosystems fisheries
301 sectors as models from other sectors usually need some basic information such as vegetation patterns
302 that are not available for natural-only conditions. The biomes models generate their own natural-only
303 vegetation patterns based on their dynamic representation of vegetation. A spin-up does not have to be
304 newly generated but is identical to the spin-up for the ‘picontrol + nat’ experiment described above.

305

306 ‘De-biased’ sensitivity simulations within the marine ecosystems and fisheries sector (FishMIP) with
307 de-biased historical oceanic forcings and no or histsoc direct human forcings (historical + nat,
308 historical + histsoc; de-biased): So far, the default oceanic forcing is not bias-adjusted as globally the
309 observational data are too sparse to be used in a similar empirical way as for the bias-adjustment of the
310 atmospheric forcing. However, the biases in the forcing are expected to also induce biases in the
311 historical and future impact simulations. To quantify these effects and to test a suggested
312 bias-adjustment method based on comprehensive ocean-biogeochemistry model simulations forced by
313 bias-adjusted atmospheric forcings we include a sensitivity experiment where the default
314 climate-related forcing is replaced by input data generated by a dynamical de-biasing approach
315 ([Lengaigne et al. 2025](#)) using the NEMO-PISCES physical-biogeochemical ocean model (Madec, 2015),
316 which is the oceanic component of the IPSL-CM6A-LR climate model. Thus, the forcing data will first be
317 generated for IPSL-CM6A-LR, but later extended to other ISIMIP-GCMs as described in subsection **2.4.2**.
318 In contrast, the oceanic forcing for the regional component of the marine ecosystems and fisheries
319 sector have been bias-adjusted by regional observational oceanic data as described in subsection **2.4.3**.
320 In this case most models only use the bias-adjusted inputs and not the raw ones. Nevertheless the
321 experiments are labeled as ‘de-biased’ sensitivity experiments to ensure a consistent naming across
322 scales.

323

324



325

326

327 **1.2 ISIMIP3b, group II: Climate-model based future impact model simulations with** 328 **constant 2015 direct human forcings**

329

330 The ISIMIP3b, group II simulations comprise a set of future impact projections (2015-2100) using fixed
331 levels of direct human forcings as considered in the historical simulations ('2015soc', '1850soc', and
332 'nat') or reached at the end (2014) of the historical period in the 'historical + histsoc' runs
333 ('2015soc-from-histsoc'). These runs are described in the red cells of **Table 4**.

334

335 **Pre-industrial reference simulations (picontrol + 2015soc, picontrol + 2015soc-from-histsoc, picontrol**
336 **+ 1850soc, picontrol + nat; default):** These simulations are included into the ISIMIP3, group II part of the
337 protocol to allow for the estimation of the effect of climate change by comparing the future impact
338 projections to simulations assuming the same background DHF but pre-industrial levels of CRF (see
339 description of baseline simulations in section 1.1).

340

341 **Future impact projections assuming SSP-RCP-based climate-related forcings starting from 'historical +**
342 **histsoc' simulations (ssp126 + 2015soc-from-histsoc, ssp370 + 2015soc-from-histsoc, ssp585 +**
343 **2015soc-from-histsoc; default):** These runs are a continuation of the group I 'historical + histsoc'
344 simulations assuming fixed 2015 direct human forcings for the future. Note that this experiment is
345 different from the experiment with fixed 2015 DHF for the future starting from the 'historical + 2015soc'
346 group I experiment (see description below).

347

348 These experiments have been introduced to describe the impacts of different scenarios of changes in
349 the climate-related systems on today's natural systems and societies, i.e. assuming present day
350 population levels and distributions, land use patterns, water, and agricultural management measures
351 etc.. In many cases, the projected changes in natural and human systems can be interpreted as the pure
352 effect of the prescribed changes in the climate-related systems. However, they could also partly result
353 from lagged effects of the historical changes in DHFs ('histsoc'), CRF ('historical'), or natural temporal
354 trends induced e.g. by re-growth of forests. To be able to separate natural trends from the effects of
355 changing CRFs, these simulations can be compared to reference impact simulations with pre-industrial
356 climate-related forcings forced with the same direct human forcings ('picontrol + 2015soc-from-histsoc',
357 see description in group I section).

358

359 **Future impact projections assuming SSP-RCP-based climate-related forcings starting from historical**
360 **simulations with constant 2015 direct human forcings (ssp126 + 2015soc, ssp370 + 2015soc, ssp585 +**
361 **2015soc; default):** These experiments continue the 'historical + 2015soc' experiments from ISIMIP3b,
362 group I using direct human forcings held constant at 2015 levels for the historical period. Although the
363 DHF in the future period is identical to the future simulations described above, the difference in
364 historical forcing may affect the impact simulations in the future period. These simulations are also
365 considered first priority as some of the impact models may not be able to handle varying direct human
366 forcings and therefore can only perform these experiments. Models participating in the



367 '2015soc-from-histsoc' experiments described above are also asked to complete the '2015soc' runs to
368 generate an as large as possible ensemble of consistent impact model simulations.

369

370 **Future impact projections assuming SSP-RCP-based climate-related forcings starting from historical**
371 **simulations assuming constant 1850 direct human forcings (ssp126 + 1850soc, ssp370 + 1850soc,**
372 **ssp585 + 1850soc; default):** These experiments continue the default 'historical + 1850soc' experiments
373 considered in ISIMIP3b, group I. They are included to estimate the impact of changes in the
374 climate-related systems conditional on 1850 levels of direct human forcings that can be compared to the
375 impact conditional on today's levels of direct human forcings ('2015soc').

376

377 **Future impact projections assuming SSP-RCP-based climate-related forcings starting from historical**
378 **simulations assuming no direct human forcings (ssp126 + nat, ssp370 + nat, ssp585 + nat; default):**
379 These experiments continue the default 'historical + nat' experiments in ISIMIP3b, group I. They are
380 included to estimate the effect of changes in the climate-related systems (here climate change itself and
381 increasing CO₂ concentrations) assuming no direct human forcings.

382

383 **CO₂ sensitivity simulations (ssp126 + 2015soc-from-histsoc, ssp370 + 2015soc-from-histsoc, ssp585 +**
384 **2015soc-from-histsoc, ssp585 + 2015soc, ssp585 + 1850soc, ssp585 + nat; 2015co2):** To separate the
385 effects of increasing atmospheric CO₂ concentrations from the effects of other changes in the
386 climate-related systems, the ISIMIP3b protocol includes sensitivity experiments where atmospheric CO₂
387 concentrations are held constant at 2015 levels. For SSP1-2.6 and SSP3-7.0, they are only introduced as
388 deviations from the default '2015soc-from-histsoc' experiments while for SSP5-8.5 the effect can also be
389 quantified conditional on all levels of direct human influences considered in the previous experiments.

390 **Future lightning sensitivity simulations (ssp126 + 2015soc-from-histsoc, ssp370 +**
391 **2015soc-from-histsoc, ssp585 + 2015soc-from-histsoc; varlightning):** To study the effects of future
392 changes in lightning flash rates as opposed to using a stationary lightning climatology, the ISIMIP3b
393 protocol includes sensitivity experiments where future lightning flash rates change along the RCPs. The
394 future lightning data sensitivity experiment is introduced as a deviation from the default
395 '2015soc-from-histsoc' experiment and only for one climate model (UK-ESM). This sensitivity
396 experiment has been introduced for the fire sector.

397 **Climate sensitivity simulations under high levels of CO₂ (ssp126 + 2015soc-from-histsoc, ssp585co2):**
398 To study the effects of high atmospheric CO₂ concentration without accompanying changes in climate,
399 the ISIMIP3b protocol includes a sensitivity experiment where the atmospheric CO₂ concentration are
400 prescribed according to RCP8.5, while the other climate-related forcings, in particular the atmospheric
401 forcings are from SSP1-2.6. The future climate sensitivity experiment is introduced as a deviation from
402 the default 'ssp126 + 2015soc-from-histsoc' experiment. This sensitivity experiment has been
403 introduced for the peat sector.

404 **'De-biased' sensitivity simulations within the marine ecosystems and fisheries sector (FishMIP) with**
405 **de-biased oceanic forcings and no or 2015soc direct human forcings for reference simulations based**
406 **on pre-industrial oceanic forcing (picontrol + nat, picontrol + 2015soc-from-histsoc; de-biased) and the**



407 associated simulations accounting for different levels of climate change (ssp126 + nat, ssp370 + nat,
408 ssp858 + nat, ssp126 + 2015soc-from-histsoc, ssp370 + 2015soc-from-histsoc, ssp585 +
409 2015soc-from-histsoc): These simulations represent the future extensions of the ‘de-biased’ group I
410 simulations described above. They are designed to test the dynamical bias-adjustment suggested for the
411 global oceanic forcings under different levels of climate change (ssp126, ssp370, ssp585). The regional
412 impact projections within the sector are also based on de-biased oceanic forcings and are therefore also
413 labeled as ‘de-biased’ sensitivity experiments to ensure a consistent labeling across scales.
414
415

Experiment	Short description	Period: Pre-industrial 1601-1849	Period: Historical 1850-2014	Period: Future 2015-2100
pre-industrial control	CRF: No changes in the climate-related systems, CO ₂ and CH ₄ fixed at 1850 levels	picontrol	picontrol	picontrol
2015soc-from-hist soc				
1st priority	DHF: Varying management before 2015, then fixed at 2015 levels thereafter	1850soc	histsoc	2015soc-from-histsoc
pre-industrial control	CRF: No changes in the climate-related systems, CO ₂ and CH ₄ fixed at 1850 levels	Does not have to be simulated as the following periods already provide 251 simulation years assuming stable baseline CRF and DHF. ensi	picontrol	picontrol
2015soc				
1st priority	DHF: Fixed at 2015 levels for all periods		2015soc	2015soc
pre-industrial control	CRF: No changes in the climate-related systems, CO ₂ and CH ₄ fixed at 1850 levels	Does not have to be simulated as the following periods already provide 251 simulation years assuming stable baseline CRF and DHF.	picontrol	picontrol
1850soc				
2nd priority	DHF: Fixed at 1850 levels for all periods		1850soc	1850soc



pre-industrial control nat 2nd priority	CRF: No changes in the climate-related systems, CO ₂ and CH ₄ fixed at 1850 levels	Does not have to be simulated as the following periods already provide 251 simulation years assuming stable baseline CRF and DHF.	picontrol	picontrol
	DHF: No direct human influences		nat	nat
RCP2.6 2015soc-from-hist soc 1st priority	CRF: Simulated historical changes in climate-related systems, CO ₂ and CH ₄ concentrations as observed in the historical period, then simulated SSP1-2.6 changes in the climate-related systems	Identical to picontrol + 1850soc run described above	historical	ssp126
	DHF: Varying management before 2015, then fixed at 2015 levels thereafter		histsoc	2015soc-from-histsoc
RCP2.6 2015soc 1st priority	CRF: Simulated historical changes in climate-related systems, CO ₂ and CH ₄ concentrations as observed in the historical period, then simulated SSP1-2.6 changes in the climate-related systems	Identical to “picontrol + 2015soc” run	historical	ssp126
	DHF: Fixed at 2015 levels for all periods		2015soc	2015soc
RCP2.6 1850soc 2nd priority	CRF: Simulated historical changes in climate-related systems, CO ₂ and CH ₄ concentrations as observed in the	Identical to “picontrol + 1850soc” run	historical	ssp126



	historical period, then simulated SSP1-2.6 changes in the climate-related systems			
	DHF: Fixed at 1850 levels for all periods		1850soc	1850soc
RCP2.6 nat 2nd priority	CRF: Simulated historical changes in climate-related systems, CO ₂ and CH ₄ concentrations as observed in the historical period, then simulated SSP1-2.6 changes in the climate-related systems	Identical to “picontrol + nat” run	historical	ssp126
	DHF: No direct human influences		nat	nat
CO₂ sensitivity RCP2.6 2015soc-from-hist soc 2nd priority	CRF: Simulated historical changes in climate-related systems, CO ₂ and CH ₄ concentrations as observed in the historical period, then simulated SSP1-2.6 changes in the climate-related systems but fixed 2015 CO ₂ concentrations	Identical to “picontrol + 1850soc” run	"histsoc" version of the historical period of the RCP2.6 experiment, as described above	ssp126 Sensitivity experiment: 2015co2
	DHF: Varying management before 2015, then fixed at 2015 levels thereafter			2015soc-from-histsoc
RCP7.0	CRF: Simulated historical changes in climate-related systems, CO ₂ and CH ₄	Identical to “picontrol + 1850soc” run	"histsoc" version of the historical period of the	ssp370



2015soc-from-hist soc 1st priority	concentrations as observed in the historical period, then simulated SSP3-7.0 changes in the climate-related systems		RCP2.6 experiment	
	DHF: Varying management before 2015, then fixed at 2015 levels thereafter			2015soc-from-histsoc
RCP7.0 2015soc 1st priority	CRF: Simulated historical changes in climate-related systems, CO ₂ and CH ₄ concentrations as observed in the historical period, then simulated SSP3-7.0 changes in the climate-related systems	Identical to “picontrol + 2015soc” run	Identical to “historical + 2015soc” run described above	ssp370
	DHF: Fixed at 2015 levels for all periods			2015soc
RCP7.0 1850soc 2nd priority	CRF: Simulated historical changes in climate-related systems, CO ₂ and CH ₄ concentrations as observed in the historical period, then simulated SSP3-7.0 changes in the climate-related systems	Identical to “picontrol + 1850soc” run	Identical to “historical + 1850soc” run described above	ssp370
	DHF: Fixed at 1850 levels for all periods			1850soc



RCP7.0 nat 2nd priority	CRF: Simulated historical changes in climate-related systems, CO ₂ and CH ₄ concentrations as observed in the historical period, then simulated SSP3-7.0 changes in the climate-related systems	Identical to “picontrol + nat” run	Identical to "historical + nat" run described above	ssp370
	DHF: No direct human influences			nat
CO₂ sensitivity RCP7 2015soc-from-hist soc 2nd priority	CRF: Simulated historical changes in climate-related systems, CO ₂ and CH ₄ concentrations as observed in the historical period, then simulated SSP3-7.0 changes in the climate-related systems but CO ₂ concentrations fixed at 2015 levels	Identical to “picontrol + 1850soc” run	Identical to "historical + histsoc" run described above	ssp370 Sensitivity experiment: 2015co2
	DHF: Varying management before 2015, then fixed at 2015 levels thereafter			2015soc-from-histsoc
RCP8.5 2015soc-from-hist soc 1st priority	CRF: Simulated historical changes in climate-related systems, CO ₂ and CH ₄ concentrations as observed in the historical period, then simulated SSP5-8.5 changes in	Identical to “picontrol + 1850soc” run	Identical to "historical + histsoc" run described above	ssp585



	the climate-related systems			
	DHF: Varying management before 2015, then fixed at 2015 levels thereafter			2015soc-from-histsoc
RCP8.5 2015soc 1st priority	CRF: Simulated historical changes in climate-related systems, CO ₂ and CH ₄ concentrations as observed in the historical period, then simulated SSP5-8.5 changes in the climate-related systems	Identical to “picontrol + 2015soc” run	Identical to “historical + 2015soc” run described above	ssp585
	DHF: Fixed at 2015 levels for all periods			2015soc
RCP8.5 1850soc 2nd priority	CRF: Simulated historical changes in climate-related systems, CO ₂ and CH ₄ concentrations as observed in the historical period, then simulated SSP5-8.5 changes in the climate-related systems	Identical to “picontrol + 1850soc” run	Identical to “historical + 1850soc” run described above	ssp585
	DHF: Fixed at 1850 levels for all periods			1850soc
RCP8.5 nat 2nd priority	CRF: Simulated historical changes in climate-related systems, CO ₂ and CH ₄ concentrations as observed in the historical period,	Identical to “picontrol + nat” run	Identical to “historical + nat” run	ssp585



	then simulated SSP5-8.5 changes in the climate-related systems			
	DHF: No direct human influences			nat
CO₂ sensitivity RCP8.5 2015soc-from-hist soc 1st priority	CRF: Simulated historical changes in climate-related systems, CO ₂ and CH ₄ concentrations as observed in the historical period, then simulated SSP5-8.5 changes in the climate-related systems but CO ₂ concentrations fixed at 2015 levels	Identical to “picontrol + 1850soc” run	Identical to "historical + histsoc" run	ssp585 Sensitivity experiment: 2015co2
	DHF: Varying management before 2015, then fixed at 2015 levels thereafter			2015soc-from-histsoc
CO₂ sensitivity RCP8.5 2015soc 1st priority	CRF: Simulated historical changes in climate-related systems, CO ₂ and CH ₄ concentrations as observed in the historical period, then simulated SSP5-8.5 changes in the climate-related systems, but CO ₂ concentrations fixed at 2015 levels	Identical to “picontrol + 2015soc” run	Identical to "historical + 2015soc" run	ssp585 Sensitivity experiment: 2015co2
	DHF: Fixed at 2015 levels for all periods			2015soc



CO₂ sensitivity RCP8.5 1850soc 2nd priority	CRF: Simulated historical changes in climate-related systems, CO ₂ and CH ₄ concentrations as observed in the historical period, then simulated SSP5-8.5 changes in the climate-related systems, but CO ₂ concentrations fixed at 2015 levels	Identical to “picontrol + 1850soc” run	Identical to "historical + 1850soc" run	ssp585 Sensitivity experiment: 2015co2
	DHF: Fixed at 1850 levels for all periods			1850soc
CO₂ sensitivity RCP8.5 nat 1st priority	CRF: Simulated historical changes in climate-related systems, CO ₂ and CH ₄ concentrations as observed in the historical period, then simulated SSP5-8.5 changes in the climate-related systems, but CO ₂ concentrations fixed at 2015 levels	Identical to “picontrol + nat” run	Identical to "historical + nat" run	ssp585 Sensitivity experiment: 2015co2
	DHF: No direct human influences			nat
Lightning sensitivity RCP2.6 2015soc-from-hist soc 2nd priority	CRF: Simulated historical changes in climate-related systems, CO ₂ and CH ₄ concentrations as observed in the historical period, then simulated SSP1-2.6 changes in the climate-related systems including	Identical to “picontrol + 1850soc” run	Identical to "historical + histsoc" run	ssp126 Sensitivity experiment: varlightning



	future lightning which in the default case is considered fixed at climatological levels			
	DHF: Varying management before 2015, then fixed at 2015 levels thereafter			2015soc-from-histsoc
Lightning sensitivity RCP7.0 2015soc-from-hist soc 2nd priority	CRF: Simulated historical changes in climate-related systems, CO ₂ and CH ₄ concentrations as observed in the historical period, then simulated SSP3-7.0 changes in the climate-related systems including future lightning which in the default case is considered fixed at climatological levels	Identical to “picontrol + 1850soc” run	Identical to "historical + histsoc" run	ssp370 Sensitivity experiment: varlightning
	DHF: Varying management before 2015, then fixed at 2015 levels thereafter			2015soc-from-histsoc
Lightning sensitivity RCP8.5 2015soc-from-hist soc 2nd priority	CRF: Simulated historical changes in climate-related systems, CO ₂ and CH ₄ concentrations as observed in the historical period, then simulated SSP5-8.5 changes in the climate-related systems including future lightning which in the default	Identical to “picontrol + 1850soc” run	Identical to "historical + histsoc" run	ssp585 Sensitivity experiment: varlightning



	case is considered fixed at climatological levels			
	DHF: Varying management before 2015, then fixed at 2015 levels thereafter			2015soc-from-histsoc
Climate sensitivity, RCP2.6 with RCP8.5 CO₂ 2015soc-from-hist soc 2nd priority	CRF: Simulated historical changes in climate-related systems, CO ₂ and CH ₄ concentrations as observed in the historical period, then CO ₂ evolves according to SSP5-8.5 while all other CRFs change according to default SSP1-2.6 forcing data	Identical to “picontrol + 1850soc” run	Identical to "historical + histsoc" run	ssp126 Sensitivity experiment: ssp585co2
	DHF: Varying management before 2015, then fixed at 2015 levels thereafter			2015soc-from-histsoc
Bias sensitivity, de-biased oceanic data for pre-industrial control	CRF: De-biased pre-industrial oceanic forcing, CO ₂ fixed at 1850 levels	Not covered	picontrol	picontrol Sensitivity experiment: de-biased
nat 2nd priority	DHF: no direct human influences	Not covered	nat	nat
Bias sensitivity, de-biased oceanic data for SSP1-2.6 nat	CRF: De-biased simulated historical oceanic forcing, then de-biased simulated SSP1-2.6 oceanic forcing	Not covered	historical	ssp126 Sensitivity experiment: de-biased
2nd priority	DHF: no direct human influences	Not covered	nat	nat



Bias sensitivity, de-biased oceanic data for SSP3-7.0 nat 2nd priority	CRF: De-biased simulated historical oceanic forcing, then de-biased simulated SSP3-7.0 oceanic forcing	Not covered	historical	ssp370 Sensitivity experiment: de-biased
	DHF: no direct human influences	Not covered	nat	nat
Bias sensitivity, de-biased oceanic data for SSP5-8.5 nat 2nd priority	CRF: De-biased simulated historical oceanic forcing, then de-biased simulated SSP5-8.5 oceanic forcing	Not covered	historical	ssp585 Sensitivity experiment: de-biased
	DHF: No direct human influences	Not covered	nat	nat
Bias sensitivity, de-biased oceanic data for pre-industrial control 2015soc-from-hist soc 2nd priority	CRF: De-biased pre-industrial oceanic forcing, CO ₂ fixed at 1850 levels	Not covered	picontrol	picontrol Sensitivity experiment: de-biased
	DHF: Varying direct human influences before 2015, then fixed at 2015 levels thereafter	Not covered	histsoc	2015soc-from-histsoc
Bias sensitivity, de-biased oceanic data for SSP1-2.6 2015soc-from-hist soc 2nd priority	CRF: De-biased simulated historical oceanic forcing, then de-biased simulated SSP1-2.6 oceanic forcing	Not covered	historical	ssp126 Sensitivity experiment: de-biased
	DHF: Varying direct human influences before 2015, then fixed at 2015 levels thereafter	Not covered	histsoc	2015soc-from-histsoc



Bias sensitivity, de-biased oceanic data for SSP3-7.0 2015soc-from-hist soc 2nd priority	CRF: De-biased simulated historical oceanic forcing, then de-biased simulated SSP3-7.0 oceanic forcing	Not covered	historical	ssp370 Sensitivity experiment: de-biased
	DHF: Varying direct human influences before 2015, then fixed at 2015 levels thereafter	Not covered	histsoc	2015soc-from-histsoc
Bias sensitivity, de-biased oceanic data for SSP5-8.5 2015soc-from-hist soc 2nd priority	CRF: De-biased simulated historical oceanic forcing, then de-biased simulated SSP5-8.5 oceanic forcing	Not covered	historical	ssp585 Sensitivity experiment: de-biased
	DHF: Varying direct human influences before 2015, then fixed at 2015 levels thereafter	Not covered	histsoc	2015soc-from-histsoc

Table 2: ISIMIP3b climate-model based experiments. The table provides a comprehensive list of all ISIMIP3b, group I (grey) and group II (red) experiments defined by the assumed climate-related forcings (CRF) and direct human forcings (DHF). Here the climate-related forcings are only described by the climate (oceanic and atmospheric) and CO₂ forcings as we do not provide coastal water levels yet.

420

421

422 2 Climate-related forcing data

423

424 2.1 Bias-adjusted and statistically downscaled atmospheric climate forcing

425

426 For ISIMIP3b we provide the daily atmospheric forcings for the same variables as in ISIMIP3a on the
 427 default 0.5° grid (see **Table 3**). These variables are from the output of CMIP6 climate model simulations,
 428 selected and processed as described below. We use the climate simulations from the picontrol (for
 429 pre-industrial conditions), historical (for historical conditions), ssp126, ssp370, and ssp585 (for future
 430 conditions under the scenarios SSP1-2.6, SSP3-7.0, and SSP5-8.5, respectively) CMIP6 experiments.

431

432



Table 3: Climate-related atmospheric forcing data provided within ISIMIP3b. The upper limits of pr and prsn correspond to 600 mm day⁻¹ and 300 mm day⁻¹, respectively, while the lower and upper limits of tas, tasmax and tasmin correspond to −90°C and +70°C, respectively.

Variable	Variable specifier	Unit (maximum range, inner bounds if considered)	Resolution	Datasets
Near-Surface Relative Humidity	hurs	% ([1, 100], [0.01, 99.99])	0.5° grid, daily	Bias-adjusted and downscaled from GFDL-ESM4, IPSL-CM6A-LR, MPI-ESM1-2-HR, MRI-ESM2-0, and UKESM1-0-LL simulations generated for CMIP6.
Near-Surface Specific Humidity	huss	kg kg ⁻¹ ([0.0000001, 0.1])	0.5° grid, daily	Derived from bias-adjusted and downscaled hurs, ps, and tas from GFDL-ESM4, IPSL-CM6A-LR, MPI-ESM1-2-HR, MRI-ESM2-0, and UKESM1-0-LL simulations generated for CMIP6.
Precipitation (including snowfall)	pr	kg m ⁻² s ⁻¹ ([0, 600/86400], [0.1/86400, ∞])	0.5° grid, daily	Bias-adjusted and downscaled from GFDL-ESM4, IPSL-CM6A-LR, MPI-ESM1-2-HR, MRI-ESM2-0, and UKESM1-0-LL simulations generated for CMIP6.
Snowfall	prsn	kg m ⁻² s ⁻¹ ([0, 300/86400]) Maximum range and inner bounds of unitless snowfall ratio (prsnratio = prsn/pr): ([0,1], [0.0001,0.9999])	0.5° grid, daily	Derived from bias-adjusted and downscaled pr and prsnratio from GFDL-ESM4, IPSL-CM6A-LR, MPI-ESM1-2-HR, MRI-ESM2-0, and UKESM1-0-LL simulations generated for CMIP6.
Surface Air Pressure	ps	Pa ([480, 110000])	0.5° grid, daily	Bias-adjusted and downscaled from GFDL-ESM4, IPSL-CM6A-LR, MPI-ESM1-2-HR, MRI-ESM2-0, and UKESM1-0-LL simulations generated for CMIP6.
Surface Downwelling Longwave Radiation	rlds	W m ⁻² ([40, 600])	0.5° grid, daily	Bias-adjusted and downscaled from GFDL-ESM4, IPSL-CM6A-LR, MPI-ESM1-2-HR, MRI-ESM2-0, and UKESM1-0-LL simulations generated for CMIP6.



Surface Downwelling Shortwave Radiation	rsds	W m ⁻² ([0, 500]) Maximum range and inner bounds of normalized rsds used during bias adjustment: ([0,1], [0.0001, 0.9999])	0.5° grid, daily	Bias-adjusted and downscaled from GFDL-ESM4, IPSL-CM6A-LR, MPI-ESM1-2-HR, MRI-ESM2-0, and UKESM1-0-LL simulations generated for CMIP6.
Near-Surface Wind Speed	sfcwind	m s ⁻¹ ([0.1, 50], [0.01, ∞])	0.5° grid, daily	Bias-adjusted and downscaled from GFDL-ESM4, IPSL-CM6A-LR, MPI-ESM1-2-HR, MRI-ESM2-0, and UKESM1-0-LL simulations generated for CMIP6.
Near-Surface Air Temperature	tas	K ([183.15, 343.15])	0.5° grid, daily	Bias-adjusted and downscaled from GFDL-ESM4, IPSL-CM6A-LR, MPI-ESM1-2-HR, MRI-ESM2-0, and UKESM1-0-LL simulations generated for CMIP6.
Daily Maximum Near-Surface Air Temperature	tasmax	K ([183.15, 343.15]) Maximum range and inner bounds considered for tasrange: ([0.01, ∞[, [0.01, ∞]) Maximum range and inner bounds considered for unitless tasskew: ([0,1], [0.0001,0.9999])	0.5° grid, daily	Derived from bias-adjusted and downscaled tasrange = tasmax - tasmin and tasskew = (tas - tasmin) / (tasmax - tasmin) from GFDL-ESM4, IPSL-CM6A-LR, MPI-ESM1-2-HR, MRI-ESM2-0, and UKESM1-0-LL simulations generated for CMIP6.
Daily Minimum Near-Surface Air Temperature	tasmin	K ([183.15, 343.15]) Maximum range and inner bounds considered for tasrange: ([0.01, ∞[, [0.01, ∞]) Maximum range and inner bounds considered for unitless tasskew: ([0,1], [0.0001,0.9999])	0.5° grid, daily	Derived from bias-adjusted and downscaled tasrange = tasmax - tasmin and tasskew = (tas - tasmin) / (tasmax - tasmin) from GFDL-ESM4, IPSL-CM6A-LR, MPI-ESM1-2-HR, MRI-ESM2-0, and UKESM1-0-LL simulations generated for CMIP6.



For the pre-industrial conditions, 500 years of picontrol output data are used and harmonised across General Circulation Models (GCM) with respect to the time range they cover. This is possible because picontrol data only carry nominal year labels. We shift the GCM-specific picontrol time ranges listed in **Table 4** to 1601–2100. For the historical and future climate conditions, we provide input data for 1850–2014 and 2015–2100, respectively, in line with the time ranges covered by the corresponding CMIP6 experiments. The common time axis is important as the use of the input data should be harmonised across all sectors. In particular, the year-by-year combination of the pre-industrial climate-related forcing with the historical direct human forcing should be done in the same way across all sectors and models.

446

Selection of climate models. To limit the number of mandatory impact simulations and hence lower the barrier to participation in ISIMIP3b, we provide climate input data for only five selected CMIP6 climate models. The basic characteristics of the five GCMs are listed in **Table 4**. The models were selected based on data availability at the selection time (late 2019 to early 2020), performance in the historical period, structural independence, process representation and equilibrium climate sensitivity (ECS).

452

To be included in ISIMIP3b, a GCM had to provide daily data for all variables listed in **Table 3** except for huss (which was derived from hurs, ps and tas, see below), ps if sea level pressure (psl) was available, so a proxy for ps could be computed based on psl and tas, and sfcwind if zonal and meridional near-surface wind components (uas, vas) were available, so a proxy for sfcwind could be computed based on uas and vas. Those daily data had to cover 500 picontrol years and all years of the historical, SSP1-2.6, SSP3-7.0, and SSP5-8.5. In addition, we favoured GCMs that provided the additional input data needed for the tropical cyclone modelling (**Table 5**) and the fisheries and marine ecosystems sector (FishMIP; **Table 10**).

460

Table 4: Characteristics of CMIP6 climate models used in ISIMIP3b. Columns show (from left to right) the climate model acronym, the horizontal grid size (longitude x latitude) of the original atmospheric output data, the ensemble member used, the nominal time range covered by the picontrol data used, the equilibrium climate sensitivity (ECS) according to (Meehl et al., 2020), and the main model reference paper and the CMIP6 simulation data publications used. For definitions of climate model acronyms and modelling groups see (Durack, n.d.).

GCM	Grid size	Member	picontrol	ECS	References
GFDL-ESM4	288 x 180	r1i1p1f1	0001–0500	2.6°C	(Dunne et al., 2020; John et al., 2018; Krasting et al., 2018)
IPSL-CM6A-LR	144 x 143	r1i1p1f1	1870–2369	4.6°C	(Boucher et al., 2018, 2019, 2020)
MPI-ESM1-2-HR	384 x 192	r1i1p1f1	1850–2349	3.0°C	(Jungclaus et al., 2019; Mauritsen et al., 2019; Schupfner et al., 2019)
MRI-ESM2-0	320 x 160	r1i1p1f1	1850–2349	3.2°C	(Yukimoto, Kawai, et al., 2019; Yukimoto, Koshiro, et al., 2019a, 2019b)



UKESM1-0-LL	192 x 144	r1i1p1f2	1960–2459	5.3°C	(Good et al., 2019; Sellar et al., 2019; Tang et al., 2019)
-------------	-----------	----------	-----------	-------	---

According to a skill analysis (see **Figure 2**), the GCMs ACCESS-CM2, AWI-CM-1-1-MR, CESM2, CESM2-WACCM, CMCC-ESM2, EC-Earth3-AerChem, GFDL-CM4, GFDL-ESM4, HadGEM3-GC31-LL, HadGEM3-GC31-MM, MPI-ESM1-2-HR, MPI-ESM1-2-LR, MRI-ESM2-0, NorESM2-MM, SAM0-UNICON, TaiESM1, and UKESM1-0-LL perform relatively well in reproducing the main historically observed characteristics of the atmosphere. From that list, only GFDL-ESM4, MPI-ESM1-2-HR, MRI-ESM2-0, and UKESM1-0-LL provided all required daily data at the time of model selection. Another model that fulfilled all those data requirements and shows an average performance in the historical period is IPSL-CM6A-LR. These five GCMs were selected to be used in ISIMIP3b. With the exception of GFDL-ESM4, these models also provide the data needed for tropical cyclone modelling. GFDL-ESM4 is the model providing the most comprehensive oceanic bio-geochemical forcings for FishMIP while other models cover less and partly other oceanic variables (see **Table 16**). Three of the climate models (GFDL-ESM4, IPSL-CM6A-LR, UKESM1-0-LL) are successors of models already used in ISIMIP2b and in the ISIMIP Fast Track.

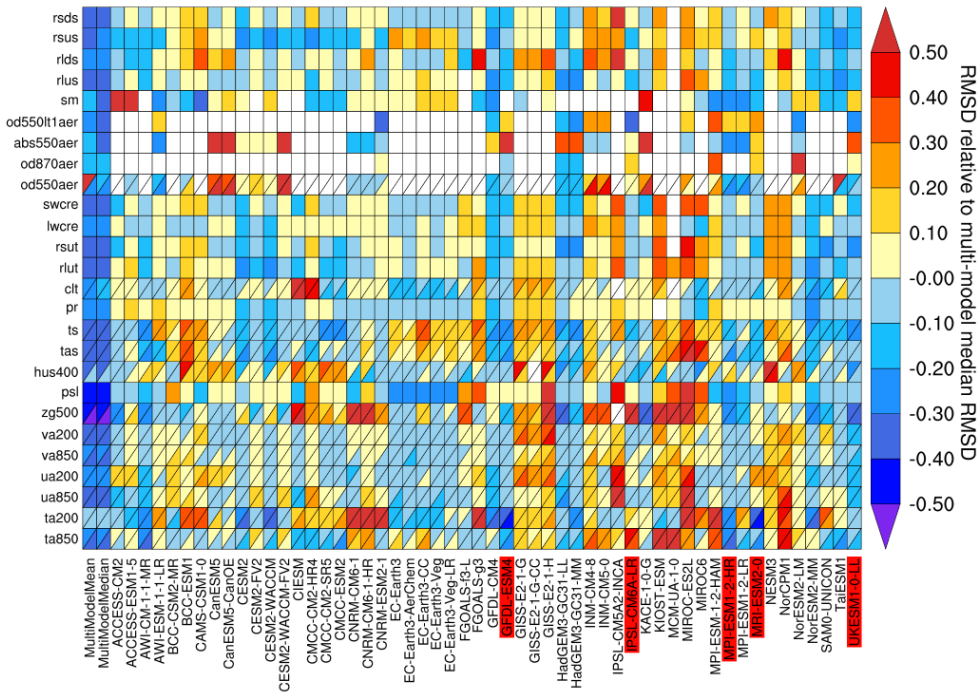


Figure 2: Relative space-time root-mean-square deviation (RMSD) calculated from the climatological seasonal cycle of the CMIP6 historical simulations (1980–1999) compared to observational datasets, for various CMIP6 GCMs (columns) and climate variables (rows), similar to Fig. 6 of (Bock et al., 2020). A relative performance is



488 displayed, with blue shading being better and red shading worse than the median RMSD of all model results of
489 the CMIP6 ensemble. A diagonal split of a grid square shows the relative error with respect to the reference data
490 set (lower right triangle) and an alternative data set (upper left triangle), as listed in Table 5 of (Bock et al., 2020).
491 White boxes are used when data are not available for a given model and variable. Models selected for ISIMIP3b
492 are highlighted in red. Variables are (from top to bottom): Surface Downwelling Shortwave Radiation (rsds),
493 Surface Upwelling Shortwave Radiation (rsus), Surface Downwelling Longwave Radiation (rlds), Surface Upwelling
494 Longwave Radiation (rlus), Soil Moisture (sm), Ambient Fine Aerosol Optical Depth at 550 nm (od550lt1aer),
495 Ambient Aerosol Absorption Optical Thickness at 550 nm (abs550aer), Ambient Aerosol Optical Depth at 870 nm
496 (od870aer), Ambient Aerosol Optical Thickness at 550 nm (od550aer), Shortwave Cloud Radiative Effect (swcre),
497 Longwave Cloud Radiative Effect (lwcre), Top-of-Atmosphere Outgoing Shortwave Radiation (rsut),
498 Top-of-Atmosphere Outgoing Longwave Radiation (rlut), Total Cloud Cover Percentage (clt), Precipitation (pr),
499 Surface Temperature (ts), Near-Surface Air Temperature (tas), Specific Humidity at 400 hPa (hus400), Sea Level
500 Pressure (psl), Geopotential Height at 500 hPa (zg500), Northward Wind at 200 hPa (va200), Northward Wind at
501 850 hPa (va850), Eastward Wind at 200 hPa (ua200), Eastward Wind at 850 hPa (ua850), Air Temperature at 200
502 hPa (ta200), and Air Temperature at 850 hPa (ta850). Produced with ESMValTool v2.0 (Andela, Broetz, de Mora,
503 Drost, Eyring, et al., 2020; Andela, Broetz, de Mora, Drost, Weigel, et al., 2020; Righi et al., 2020) .

504

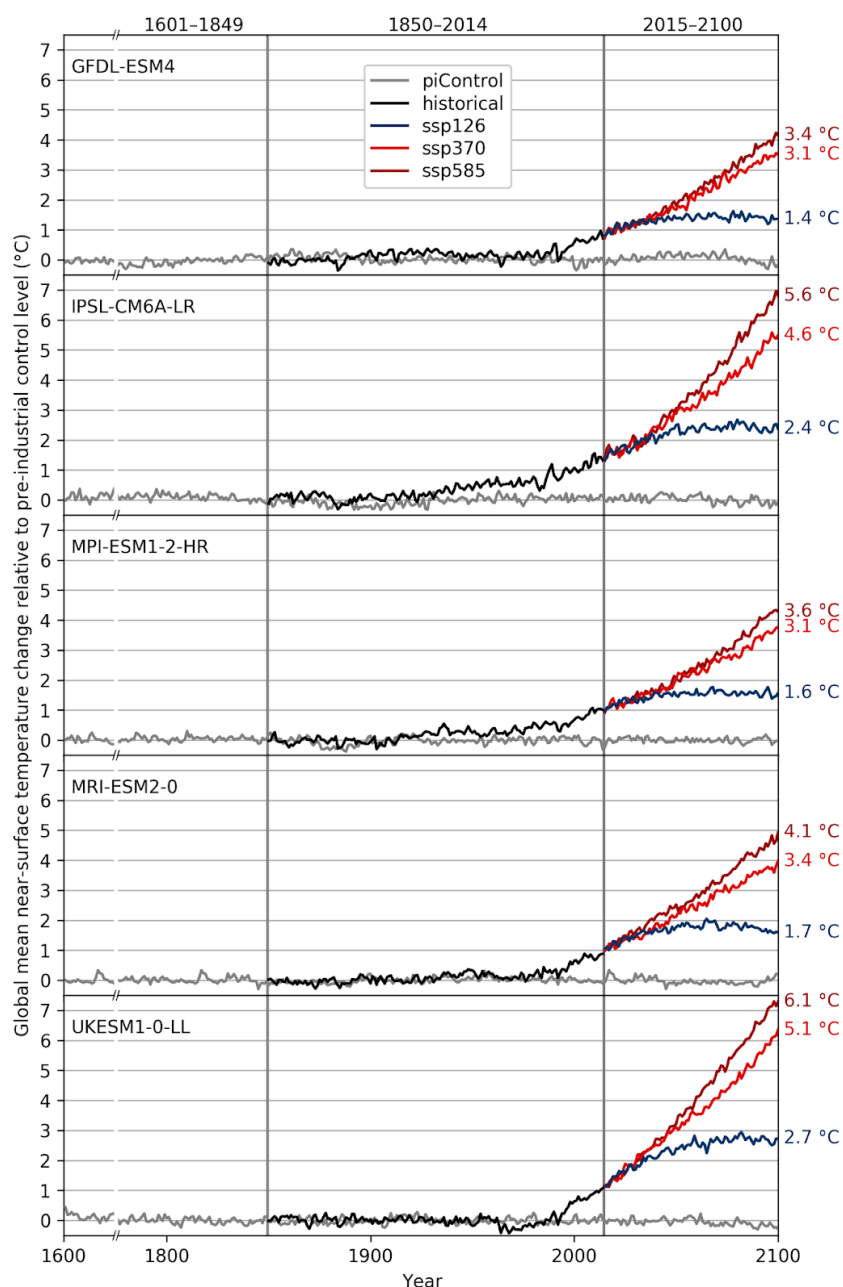
505

506 The five GCMs are structurally independent in terms of their ocean and atmosphere model components.
507 Furthermore, all of them have a coupled climate and carbon cycle and in some cases, fully interactive
508 chemistry and aerosol components. We favoured models that applied prognostic couplings between
509 processes and model domains wherever possible to maximise the coverage of simulated feedbacks.

510

511 The five GCMs provide a good representation of both the mean and the range of the full CMIP6
512 multi-model ensemble ECS. According to (Meehl et al., 2020), the CMIP6 multi-model mean ECS is 3.7°C
513 , which is precisely met by the mean ECS of the five ISIMIP3b GCMs. The transient climate response
514 (TCR) of 2.0°C is also precisely met. This provides an improvement over ISIMIP2b. In that case the mean
515 ECS for the full CMIP5 was 3.2°C compared with a mean ECS of 3.72°C for the four ISMIP2b GCMs (see
516 Table S1 and S2 in (Jägermeyr et al., 2021)). The ISIMIP3b ensemble includes three models with
517 below-average ECS (GFDL-ESM4, MPI-ESM1-2-HR, MRI-ESM2-0) and two models with above-average
518 ECS (IPSL-CM6A-LR, UKESM1-0-LL) (see **Table 12**). In line with their ECS values, we find GFDL-ESM4 and
519 UKESM1-0-LL to project the weakest and strongest global warming, respectively, under any future
520 scenario considered (see **Figure 3**). Under SSP5-8.5, the global mean near-surface temperature in 2100
521 is about 3°C larger in UKESM1-0-LL than in GFDL-ESM4. Under SSP1-2.6, the projections are about 1.5°C
522 apart. The ensemble mean warming of the ISIMIP3b CMIP6 models is significantly higher than the
523 warming of the ISIMIP2b CMIP5 models, across global land area by an average of 0.3°C, but over the
524 main breadbasket cropland regions by more than 0.5°C between 1983–2013 and 2069–2099, under
525 both SSP1-2.6 and SSP5-8.5 (Table S1 in (Jägermeyr et al., 2021)).

526



527

Figure 3: Time series of annual global mean near-surface temperature change relative to pre-industrial levels (1601–1849 average) as simulated with GFDL-ESM4, IPSL-CM6A-LR, MPI-ESM1-2-HR, MRI-ESM2-0 and UKESM1-0-LL (from top to bottom). Colour coding indicates the underlying CMIP6 experiments (grey: pre-industrial control, black: historical, blue: SSP1-2.6, light red: SSP3-7.0, dark red: SSP5-8.5) with corresponding time periods given at the top. Numbers to the right of the plot represent end-of-century warming levels under the



different future scenarios, expressed as the global multi-year mean near-surface temperature change from 1601–1849 to 2070–2100.

535

Bias adjustment and statistical downscaling. To make the GCM-based climate forcing usable for the impact modellers we apply a bias adjustment ensuring that the GCM simulations match the observed distribution of climate data over the historical reference period (1979–2014). In addition to the bias adjustment a statistical downscaling to our standard 0.5° grid is included in the pre-processing of the surface and near-surface atmospheric variables (see **Table 11**). The method used for the bias adjustment and statistical downscaling (BASD) in ISIMIP3b is version 2.5 of ISIMIP3BASD (Lange, 2019b, 2021a).

542

ISIMIP3BASD has several advantages compared to the method used for bias adjustment and statistical downscaling in ISIMIP2b (Frieler et al., 2017; Lange, 2017, 2018). First, it clearly separates the adjustment of biases in climate model output at 1° or 2° resolution, whatever is closest to the original output data, from the statistical downscaling to the target resolution of 0.5°. Compared to ISIMIP2b, where climate model output was first spatially interpolated to the target resolution and then bias-adjusted, the new approach improves the spatial variability at the target resolution (Lange, 2019b). Second, the new quantile mapping method preserves trends in each quantile of the distribution of the daily data and adjusts biases in distribution quantiles of the daily data more accurately than the ISIMIP2b bias adjustment methods (Lange, 2019b).

552

For trend preservation, we first produce pseudo-future observations by shifting the historically observed daily data by the simulated future climate change. Here, the signal of climate change is the difference or the ratio between the inverse empirical cumulative distribution function of the historical period and the respective distribution functions of each 36-year period of the future. Using the difference ensures additive trend preservation and using the ratio ensures multiplicative trend preservation under bias adjustment. We apply additive trend preservation for near-surface air temperature (tas), sea level pressure (psl, see **Table 6**), and surface downwelling longwave radiation (rlds). We apply primarily multiplicative trend preservation for precipitation including snowfall (pr), near-surface wind speed (sfcWind), and the range (tasrange = tasmax - tasmin) between the daily maximum and minimum near-surface air temperatures (tasmax and tasmin, respectively) that can transition smoothly to additive trend preservation for data with large negative biases in the historical period (Lange, 2019b). In a second step, the future simulations are mapped onto the pseudo-future observations by quantile mapping. Both steps, the generation of the pseudo future observations and the quantile mapping of the future simulations onto the pseudo observations, are applied for each day of the year separately. The distributions include data from the 31 days around the considered day and all years of the reference or future period, respectively. This means a sample size of 31x36 values for each day of the year. Through this approach the bias adjustment implicitly also adjusts the multi-year mean annual cycle and a mix of year-to-year and day-to-day variability (Haerter et al., 2011).

571

In addition, the method adjusts the frequency of daily data falling outside of the inner bounds specified in **Table 11** (e.g. the dry day frequency, i.e. the number of days with precipitation below 0.1 mm day⁻¹).

574



Four variables were adjusted and downscaled indirectly: near-surface specific humidity (huss) was derived from adjusted and downscaled near-surface relative humidity (hurs), surface air pressure (ps), and near-surface air temperature (tas) using the equations of (Buck, 1981) as described in (Weedon et al., 2010), snowfall (prsn) was derived from adjusted and downscaled precipitation including snow (pr) and the snowfall ratio (prsnratio = prsn / pr), and daily maximum and daily minimum near-surface air temperatures (tasmax and tasmin, respectively) were derived from adjusted and downscaled tas, and the tasrange = tasmax - tasmin and skewness of the daily temperature cycle tasskew = (tas - tasmin) / (tasmax - tasmin).

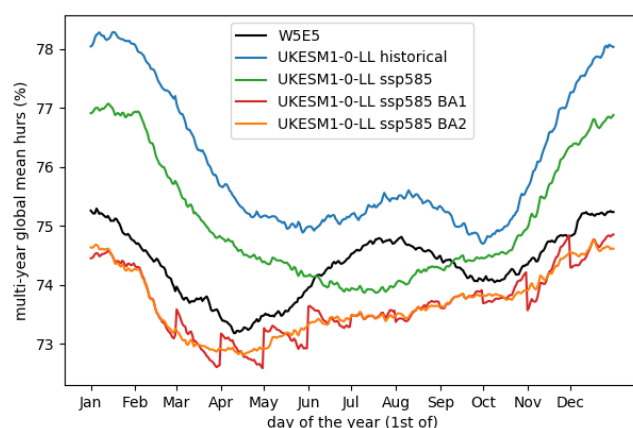
583

The basic characteristics of ISIMIP3BASD (version 1.0) are described in (Lange, 2019b). However, the method finally used to generate the forcing data now provided within ISIMIP3b (ISIMIP3BASD version 2.5) deviates from the original version in some aspects. In the following we describe the most important updates of the procedure relative to the one described in (Lange, 2019b). For a complete list of differences between the two versions of the BASD method and the full history of which feature was added in which update, see the CHANGELOG included in the archive of code version 2.5 (Lange, 2021a).

590

In (Lange, 2019b) the bias-adjustment was applied on a monthly basis, i.e. the pseudo-future observations and the quantile mapping described above was applied to all daily January data, February data and so forth. This approach can introduce discontinuities at the transition from one month to another (see **Figure 4**). That is why for ISIMIP3b the adjustment is done in the running window mode with steps of one day and a window width of 31 days as described above. This approach resolves the discontinuity issue (see **Figure 4**), as suggested by (Thiemeßl et al., 2012); (Thrasher et al., 2012); (Gennaretti et al., 2015); and (Grenier, 2018).

598



599

Figure 4: Global multi-year daily mean near-surface relative humidity for UKESM1-0-LL historical (1979-2014) and SSP5-8.5 (2065-2100), with historical simulated data in blue, future simulated data in green, future bias-adjusted data in red and orange, and observational reference data in black. A smooth annual cycle is produced if ISIMIP3BASD v2.5 is applied in running-window mode in steps of one day (orange, BA2). In contrast, a month-by-month application, which was the only option in ISIMIP3BASD v1.0, generates discontinuities at each turn of the month (red, BA1).



606

607 Since ps, rlds and tas can show significant trends within the 36-year training and application periods
608 ISIMIP3BASD v1.0 includes a detrending of these variables within these intervals before the pseudo
609 future observations and the transfer functions are estimated and applied. Afterwards the trend is added
610 back again. This is done to prevent the confusion of trends with interannual variability during quantile
611 mapping (Lange, 2019b; Maraun, 2013). In contrast to v1.0, in v2.5, applied to generate the ISIMIP3b
612 forcings data, the detrending is only applied if the trend is significantly different from zero at the 5%
613 level.

614

615 We also changed the method used to generate future pseudo-observations of bounded variables
616 (equations (8) and (9) of (Lange, 2019b)), in order to stabilise results in some edge cases. If, e.g., the
617 historically observed relative dry-day frequency was 0.0 while the simulated frequency was 0.8 for the
618 historical period and 0.9 for some future period, then, according to equation (9) of (Lange, 2019b), the
619 future pseudo-observed frequency would be equal to $1 - (1 - 0.0)(1 - 0.9)/(1 - 0.8) = 0.5$. As
620 this is considered unrealistic we apply a revised version of equation (9) of (Lange, 2019b) that reads

621

$$\begin{aligned} 622 \quad P_{fut}^{obs} &= \{ \\ 623 \quad P_{fut}^{sim} &\text{ if } P_{hist}^{sim} = P_{hist'}^{obs} \\ 624 \quad 0 + (P_{hist}^{obs} - 0)(P_{fut}^{sim} - 0)/(P_{hist}^{sim} - 0) &\text{ if } P_{fut}^{sim} \leq P_{hist}^{sim} < P_{hist'}^{obs} \\ 625 \quad 1 - (1 - P_{hist}^{obs})(1 - P_{fut}^{sim})/(1 - P_{hist}^{sim}) &\text{ if } P_{fut}^{sim} \geq P_{hist}^{sim} < P_{hist'}^{obs} \\ 626 \quad P_{hist}^{obs} + P_{fut}^{sim} - P_{hist}^{sim} &\text{ otherwise.} \end{aligned} \quad (1)$$

627

628 In this revised relation, the otherwise case applies if $P_{fut}^{sim} < P_{hist}^{sim} < P_{hist'}^{obs}$ or
629 $P_{fut}^{sim} > P_{hist}^{sim} > P_{hist'}^{obs}$. Hence it applies to the aforementioned edge case, where it produces a less
630 extreme future pseudo-observed relative frequency of $0.0 + 0.9 - 0.8 = 0.1$. Equation (8) of
631 (Lange, 2019b) was revised analogously to equation (9).

632

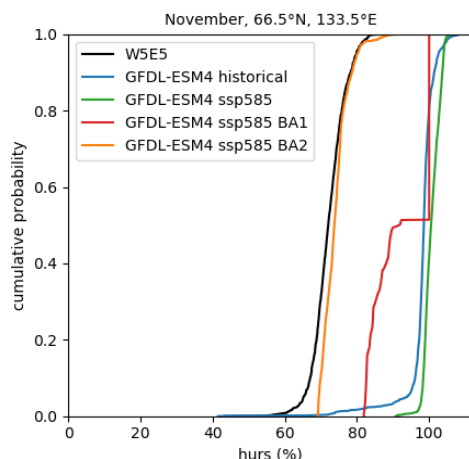
633 Furthermore, we refined the method used to generate future pseudo-observations (step 5 of the bias
634 adjustment algorithm of (Lange, 2019b)) for all variables with at least one bound: In v1.0, the future
635 pseudo observations were generated by transferring simulated trends in all distribution quantiles to the
636 observational reference data. That included trends in, e.g., precipitation quantiles below the wet-day
637 threshold. However, in some cases, the trend transfer turned many dry days into wet days, with a
638 profound impact on the shape of the distribution of future pseudo-observed wet-day precipitation. As a
639 result, simulated trends in wet-day precipitation intensity were not well preserved. In v2.5, trend
640 transfers are restricted to values within threshold. This particularly improves the preservation of trends
641 in wet-day precipitation intensities.

642



We also modified the bias adjustment method for Near-Surface Relative Humidity (hurs) because ISIMIP3BASD v1.0 turned out to produce unrealistic distributions of hurs under climate change if there are too many cases of supersaturation ($\text{hurs} \geq 100\%$) in the simulated data. This is the case for several of the CMIP6 GCMs selected for ISIMIP3b, particularly in high-latitude winter: While no supersaturations are found in the observational reference data, the GCM simulates many supersaturations in the historical reference period and even more so in a future period, under SSP5-8.5 (see Figure 5). ISIMIP3BASD v1.0 preserves this projected trend and hence produces future bias-adjusted hurs data with many supersaturations. In v2.5, this trend is no longer preserved. Instead, the supersaturation probability is fixed at the observed level, which is zero or very close to zero in all seasons and grid cells for W5E5. Future pseudo observations of hurs are generated by applying the revised (see above) equation (8) of (Lange, 2019b) to all hurs values after capping them at 100%. The new approach was motivated by findings from (Ruosteenoja et al., 2017, 2018). They analysed hurs data from CMIP5 and showed that (i) supersaturations in those data are mostly spurious, resulting from, e.g., inconsistencies in the interpolation of temperature and specific humidity to the near-surface level, and (ii) climatological mean value trends of hurs become more consistent with trends in relative humidity from the lowest model level if hurs is capped at 100% before trends are calculated.

659



660

661

Figure 5: Empirical cumulative distribution functions of near-surface relative humidity in high-latitude winter (November, 66.5°N, 133.5°E) for GFDL-ESM4 historical (1979-2014) and SSP5-8.5 (2065-2100), with historical simulated data in blue, future simulated data in green, future bias-adjusted data in red and orange, and observational reference data in black. The simulated climate change signal is well preserved with ISIMIP3BASD v2.5 using a fixed supersaturation ($\text{hurs} \geq 100\%$) probability and equation (1) applied to all hurs values after capping them at 100% to generate future pseudo observations (orange, BA2). In contrast, the simulated climate change signal is not well preserved if the supersaturation probability is allowed to change and equations (8) and (9) of (Lange, 2019b) are used to generate future pseudo observations of hurs (red, BA1).

670

In addition, while ISIMIP3BASD v1.0 applies parametric quantile mapping to all climate variables, we used a nonparametric approach for the bias adjustment of near-surface relative humidity (hurs), the



673 snowfall ratio (prsnratio), surface downwelling shortwave radiation (rsds), and the skewness of the daily
674 temperature (tasskew) since the parametric quantile mapping method previously used for those
675 variables suffered from occasionally unstable beta distribution fits.

676

677 Moreover, the parametric quantile mapping described in (Lange, 2019b) does not only adjust biases in
678 quantiles of the simulated daily data but also adjusts biases in the likelihood of individual events, as in
679 (Switanek et al., 2017). To avoid overfitting artefacts we did not adjust event likelihoods for ISIMIP3b.

680

681 Finally, the diurnal temperature range (tasrange) was ultimately bias-adjusted using a Weibull
682 distribution, not a Rice distribution as described in (Lange, 2019b) because the Weibull distribution fits
683 the data better in most cases, in particular in the upper tail.

684

685 For further details of the application of ISIMIP3BASD v2.5 for ISIMIP3b, including the exact Python
686 commands and application periods used per CMIP6 experiment, see the ISIMIP3b bias adjustment fact
687 sheet (Lange, 2021b).

688

689 In addition, we use a new observational target dataset. Instead of using the EWEMBI dataset (E2OBS,
690 WFDEI and ERAI data merged and bias-corrected for ISIMIP; (Lange, 2019a) in ISIMIP3b we adjust the
691 climate forcing data to version 2.0 of the W5E5 dataset (WFDE5 over land merged with ERA5 over the
692 ocean; (Lange et al., 2021). The data cover the entire globe at 0.5° horizontal and daily temporal
693 resolution from 1979 to 2019. W5E5 v2.0 is derived by applying version 2.0 of the WATCH Forcing Data
694 methodology (WFDE5; (Cucchi et al., 2020) to ERA5 reanalysis data (Hersbach et al., 2020) and
695 precipitation data from version 2.3 of the Global Precipitation Climatology Project (GPCP; (Adler et al.,
696 2003)).

697

698 The statistical downscaling method did not change between v1.0 and v2.5 of ISIMIP3BASD, i.e. for
699 ISIMIP3b we use the approach described (Lange, 2019b). This method adds the spatiotemporal
700 variability that is missing at the low spatial resolution at which the bias adjustment is done (1° or 2°,
701 depending on the GCM), compared to the target resolution of the downscaling (0.5°). The method is a
702 modified version of the MBCn algorithm from (Cannon, 2018), which in turn is a stochastic, multivariate,
703 non-parametric quantile mapping method. We use it to transfer the statistical relationship between
704 low-resolution and high-resolution W5E5 data to the GCM output that was previously bias-adjusted
705 using low-resolution W5E5 data. In comparison to the approach used in ISIMIP2b (a spatial interpolation
706 to the target resolution followed by a bias adjustment at that resolution), the approach used in ISIMIP3b
707 is less prone to inflate temporal variability and deflate spatial variability, i.e. the ISIMIP3b approach
708 produces more realistic spatiotemporal variability patterns at the target resolution (Lange, 2019b).

709

710 2.2 Tropical cyclones

711

712 **Table 5:** Information about tropical cyclone tracks and windfields provided as climate-related forcing
713 data within ISIMIP3b.



Variable	Variable specifier	Unit	Resolution	Datasets
Time associated with a given location of the storm centre	time	hours since 1950-01-01 00:00	along-track, 2-hourly (MIT model) 6-hourly (CHAZ model)	MIT (Emanuel et al., 2008) and CHAZ (Lee et al., 2018)
Latitudinal coordinate of storm centre	lat	degrees north	along-track, 2-hourly (MIT model) 6-hourly (CHAZ model)	MIT (Emanuel et al., 2008) and CHAZ (Lee et al., 2018)
Longitudinal coordinate of storm centre	lon	degrees east	along-track, 2-hourly (MIT model) 6-hourly (CHAZ model)	MIT (Emanuel et al., 2008) and CHAZ (Lee et al., 2018)
Central pressure	pres	hPa	along-track, 2-hourly	MIT (Emanuel et al., 2008)
Maximum 1-minute sustained wind speed	windspatialmax	knots	along-track, 2-hourly (MIT model) 6-hourly (CHAZ model)	MIT (Emanuel et al., 2008) and CHAZ (Lee et al., 2018)
Radius of maximum wind speeds	rmw	km	along-track, 2-hourly	MIT (Emanuel et al., 2008)
Wind speed on the 850 hPa pressure level	u850 v850	knots (MIT model), ms^{-1} (CHAZ model)	along-track, 2-hourly (MIT model) 6-hourly (CHAZ model)	MIT (Emanuel et al., 2008) and CHAZ (Lee et al., 2018)
Temperature on the 600 hPa pressure level	t600	K	along-track, 2-hourly (MIT model) 6-hourly (CHAZ model)	MIT (Emanuel et al., 2008) and CHAZ (Lee et al., 2018)
Frequency of TC occurrence	freqyear	count per year	annual	MIT (Emanuel et al., 2008)
Gridded lifetime maximum 1-minute sustained wind speed	windlifetimemax	ms^{-1}	Per storm on a 300 arc-seconds (~10 km) grid	Wind fields calculated with Holland and Emanuel-Rotunno wind profiles (Holland, 1980, 2008) for both sets of synthetic tracks (CHAZ and MIT)
Maximum 24-hourly rainfall total during the whole storm duration	maxrain	mm	per storm on a 300 arc-seconds (~10 km) grid	Maximum 24-hourly rainfall (Zhu et al., 2013) calculated for Holland and Emanuel-Rotunno wind profiles for both sets of synthetic tracks (CHAZ and MIT)



We provide large ensembles of potential realisations of TC tracks and intensities that are consistent with the large-scale atmospheric and oceanic conditions simulated by the 5 ISIMIP3b GCMs (see **Table 4**) and for a selection of scenarios considered in ISIMIP3b (see **Table 1**). We provide gridded wind (maximum 1-minute sustained wind speeds during the whole duration of the TC) and rainfall (maximum 24-hourly amounts of rain during the whole duration of the TC) fields at a spatial resolution of 300 arc-seconds (approximately 10 km) by the same approaches also applied to the historically observed tracks ((Frier et al., 2024), section 3.2).

The tracks are generated by two different statistical-dynamical approaches that, forced by GCM data (see **Table 4**), generate a large number of synthetic storms. Both methods to generate the TC tracks consist of a genesis, a track, and an intensity module:

The MIT approach. Within MIT (Emanuel et al., 2008), the time-evolving state of the atmosphere and ocean surface given by the GCMs is randomly (uniformly distributed in time and space) seeded by weak proto-cyclones (genesis module). The seed disturbances are assumed to move with the GCM-provided large-scale flow in which they are embedded, plus a westward and poleward component owing to planetary curvature and rotation (track module). Their intensity is calculated using the Coupled Hurricane Intensity Prediction System (CHIPS; (Emanuel et al., 2004), a simple axisymmetric hurricane model coupled to a reduced upper ocean model to account for the effects of upper ocean mixing of cold water to the surface (intensity module). Applied to the synthetically generated tracks, this model simulates which of the seeded proto-cyclones develop into TCs, reaching maximum 1-minute sustained wind speeds of at least 35 knots, or dissipate due to unfavourable environments. The probabilistic seeding of proto-cyclones is repeated until the desired number of storms per year is reached (in our case, 1500). For each year, the share of proto-cyclones that dissipated in the process is used to derive an estimate of annual TC occurrences (**freqyear**). Extensive comparisons to historical events (Emanuel et al., 2008) have revealed that the statistical properties of the simulated events are consistent with historical TC genesis.

1500 tracks were generated globally and for each year of the ISIMIP3b period 1850–2100 (except for GFDL-ESM4, where tracks were only generated for 1850-2014 and 2061-2100, and MRI-ESM2-0 for 1950-2100, see **Table 1**). Depending on the application, a simple subsampling (Meiler et al., 2022) or a more advanced bias-correction and emulation procedure (Geiger et al., 2021) might be necessary to extract properly-sized sets of potential realisations from the MIT ensembles.

The MIT track data shall be used for non-commercial research or academic purposes only. Data can be made available by the ISIMIP team upon written consent by Kerry Emanuel (MIT, email: emanuel@mit.edu).

The CHAZ approach. CHAZ (Lee et al., 2018) seed disturbances are also initialised randomly, but, in contrast to the MIT model, the global seeding rate and the local probabilities are derived from two versions of a TC genesis index (TCGI, (Tippett et al., 2011) (genesis module) and intended to represent the environmental conditions instead of being adjusted to produce a prescribed number of TCs. It is noted that CHAZ's projection of global and basin-wide TC annual frequency is sensitive to the choice of the particular variable used to represent moisture in its genesis module. Simulations using column



relative humidity (CRH) as the moisture variable tend to project an overall increase in global TC frequency, while those using saturation deficit (SD) show a decrease (Camargo et al., 2014), (Lee et al., 2020). Both parameters describe how far the atmosphere is from saturation, and they have very similar spatial patterns in the present climate, so historical data cannot be used to determine which variable is the best choice to represent the climate. These two configurations reflect the uncertainty of TC frequency projections (Sobel et al., 2021). Here we provide CHAZ downscaling using both choices of moisture variable to account for this uncertainty.

Similar to MIT, CHAZ then moves the synthetic storms by advection of the environmental steering flow plus a beta drift (track module). The evolution of synthetic storm intensity is calculated using the surrounding atmospheric conditions through an empirical multiple linear regression model plus a stochastic component (intensity module, (Lee et al., 2015, 2016)). The stochastic component accounts for internal storm dynamics that do not depend explicitly on the environment. While, in MIT, TC occurrence frequency is provided as an additional variable, in CHAZ, this information is implicitly contained in the number of TCs that were seeded by the genesis module and that reached TC strength according to the intensity module.

For ISIMIP3b, 20 different CHAZ realisations of the genesis and subsequent tracks are generated with 40 ensemble members each from the intensity module. For each of the 20 realisations, we compute wind and rain fields for the first ensemble member from the intensity ensemble. The design of 20 realisations allows CHAZ to generate similar numbers (~1800) of synthetic storms per year per GCM as the MIT models over the historical period. The exact number of storms per year in CHAZ varies by GCM, by scenario, by the choice of humidity variables in CHAZ's genesis component (Lee et al., 2020). On average, CHAZ generates 1817, 1802, 1820, 1810, 1842 storms per year for GFDL-ESM4, IPSL-CM6A-LR, MPI-ESM1-2-HR, MRI-ESM2-0, and UKESM1-0-LL, respectively. The CHAZ model has been shown to capture the statistical properties of the observed storms when forced by a global reanalysis data (Lee et al., 2018). Its CMIP6 downscaling results are reported in (Fosu et al., 2024). (Sobel et al., 2019) used both models to study cyclone risk at Mumbai, India and showed that MIT and CHAZ generate comparable return periods (frequency of exceedance) of maximum wind speeds at landfall. However, a frequency bias-correction might still be necessary, depending on the application (Meiler et al., 2022).

The track data generated by the CHAZ approach shall be used for non-commercial research or academic purposes only. Data can be made available by the ISIMIP team upon written consent by Chia-Ying Lee (Columbia University, email: cl3225@columbia.edu).

Table 6: Climate input data interpolated to 2° horizontal resolution and provided without bias adjustment for tropical cyclone modelling with MIT and CHAZ.

Variable	Variable specifier	Unit	Resolution	Datasets
Sea Water Potential Temperature	thetao	°C	2° grid, model specific levels (m from surface to 200m depth), monthly	IPSL-CM6A-LR, MPI-ESM1-2-HR, MRI-ESM2-0, and UKESM1-0-LL simulations generated for CMIP6.



Sea Surface Temperature	tos	°C	2° grid over the ocean, monthly	IPSL-CM6A-LR, MPI-ESM1-2-HR, MRI-ESM2-0, and UKESM1-0-LL simulations generated for CMIP6.
Surface Temperature	ts	K	2° grid covering land and ocean areas, monthly	IPSL-CM6A-LR, MPI-ESM1-2-HR, MRI-ESM2-0, and UKESM1-0-LL simulations generated for CMIP6. ts may differ from tos in regions of sea ice where tos refers to temperatures under the ice while ts refers to temperatures at the surface.
Air Temperature	ta	K	2° grid; 15 pressure levels (from 1000 to 30 hPa), monthly	IPSL-CM6A-LR, MPI-ESM1-2-HR, MRI-ESM2-0, and UKESM1-0-LL simulations generated for CMIP6.
Specific Humidity	hus	kg kg ⁻¹	2° grid; 15 pressure levels (from 1000 to 30 hPa), monthly	IPSL-CM6A-LR, MPI-ESM1-2-HR, MRI-ESM2-0, and UKESM1-0-LL simulations generated for CMIP6.
Relative Humidity at 600 hPa	hur	%	2° grid, monthly	IPSL-CM6A-LR, MPI-ESM1-2-HR, MRI-ESM2-0, and UKESM1-0-LL simulations generated for CMIP6.
Precipitable water (water vapour content vertically integrated through the atmospheric column)	prw	kg m ⁻²	2° grid, monthly	IPSL-CM6A-LR, MPI-ESM1-2-HR, MRI-ESM2-0, and UKESM1-0-LL simulations generated for CMIP6.
Sea Level Pressure	psl	Pa	2° grid, monthly	IPSL-CM6A-LR, MPI-ESM1-2-HR, MRI-ESM2-0, and UKESM1-0-LL simulations generated for CMIP6.
Eastward Wind	ua	m s ⁻¹	2° grid; 200, 250, 850 hPa; monthly	IPSL-CM6A-LR, MPI-ESM1-2-HR, MRI-ESM2-0, and UKESM1-0-LL simulations generated for CMIP6.
Northward Wind	va	m s ⁻¹	2° grid; 200, 250, 850 hPa; monthly	IPSL-CM6A-LR, MPI-ESM1-2-HR, MRI-ESM2-0, and UKESM1-0-LL simulations generated for CMIP6.
Eastward Wind	ua	m s ⁻¹	2° grid; 250, 850 hPa; daily	IPSL-CM6A-LR, MPI-ESM1-2-HR, MRI-ESM2-0, and UKESM1-0-LL simulations generated for CMIP6.



Northward Wind	va	m s-1	2° grid; 250, 850 hPa; daily	IPSL-CM6A-LR, MPI-ESM1-2-HR, MRI-ESM2-0, and UKESM1-0-LL simulations generated for CMIP6.
----------------	----	-------	---------------------------------	---

789

790 **2.3 Coastal water levels**

791

792 **Table 7:** Coastal water level specifications

Variable	Variable specifier	Unit	Resolution	Datasets
Coastal water levels	cwl	m	custom coastal grid Hourly or daily maxima	planned

793

794

795 We do not yet provide coastal water levels as forcing data for ISIMIP3b. However, we plan to generate
796 time series of coastal water levels from 1900 to 2100 at hourly resolution or for daily maxima. The data
797 set and method will be described in a separate manuscript. Similar to the hourly water level dataset of
798 ISIMIP3a (see section 3.3 of (Frieler et al., 2024) and (Treu et al., 2023)), we will combine longer-term
799 annual sea level change with estimates of short-term coastal water level variation. Concerning the
800 long-term sea level change component, we will further develop the ISIMIP2b approach (Frieler et al.,
801 2017) and use tide gauge, satellite, vertical land motion and global climate model data to constrain a
802 model with observations and IPCC AR6 projections in a Bayesian setting. Modelled global contributions
803 from ice sheets and fingerprints are translated to regional sea level rise via fingerprints. A new aspect is
804 that we include an estimation of vertical land motion to provide relative coastal water levels instead of
805 geocentric coastal water levels. A version of the model that projects sea level rise at tide gauge stations
806 (and not all coastlines as is needed here) is currently in review ((Perrette & Mengel, submitted 2024)).
807 We plan to estimate the short-term coastal water level variation by a machine-learning approach that is
808 trained to reproduce simulations of the Global Surge and Tide Model (GTSM) model driven by ERA5
809 reanalysis data (Muis et al., 2020) or simulations from HighResMIP (Muis et al., 2023). We are currently
810 testing the dependency of the short-term water level variation on available atmospheric information at
811 GCM resolution. If the predictive power is high enough we will use the findings to provide
812 computationally efficient water level projections specific for the ISIMIP GCMs.

813

814 **2.4 Ocean data**

815

816 In the default experiments, the ocean variables provided by the GCMs are not subject to
817 bias-adjustment, unlike the atmospheric forcing data (section 2.4.1). This is due to the absence of a
818 comprehensive global observational oceanic dataset to serve as a reference for the adjustment.



819 However, in order to mitigate potential biases in global impact model simulations stemming from biases
820 in raw oceanic forcing data, we provide a de-biased version to be used in a sensitivity experiment (see
821 **Table 2**). They will be derived from an ocean-biogeochemistry model forced by bias-adjusted monthly
822 atmospheric surface flux data from four of the five ISIMIP3b GCMs. The approach preserves the monthly
823 variability of the underlying GCM while the daily variability is added from an independent simulation
824 (see section **2.4.2**).

825 For the regional impact model simulations, observational data for individual variables have either been
826 applied directly (if the required forcing was observed) to rectify biases in regional oceanic forcings by
827 the delta method or have first been translated into the required forcing variable by model simulations
828 (see section **2.4.3**). In the delta approach absolute simulated deviations from reference levels are added
829 to the observed reference levels. The regional bias-adjustment is independent from the generation of
830 the global de-biased forcing data.

831 In order to gauge the effects of these adjustments on the corresponding impact simulations, the
832 protocol includes sensitivity experiments (**'de-biased'**) grounded on these adjusted climate-related
833 forcings (see **Table 2**). The comparison of associated impact simulation to the default ones is expected
834 to provide valuable insights into the effects of potential biases in the climate-related forcings. The
835 'de-biased' experiments are considered a starting point to develop methods to bias-adjust the oceanic
836 forcings in further ISIMIP simulation rounds and make these simulations the default ones. Following the
837 ISIMIP 'consistency framing' the bias-adjustment should also preserve the daily variability of the original
838 GCM simulations to allow for a cross-sectoral integration on daily time scale. .

839 **2.4.1 Raw data without bias adjustment (default experiment)**

840 In ISIMIP3b, a set of physical and biogeochemical ocean variables nearly identical to that in ISIMIP3a is
841 provided (see section **3.4**, **Table 8** of (Frieler et al., 2023) and **Table 8** below). These variables are
842 obtained from the CMIP6 GCMs, which also supply the atmospheric forcing for ISIMIP3b, except for
843 MRI-ESM2-0, which lacks bio-geochemical variables. In other models, only certain individual variables
844 are missing (see **Table 8**). Obtaining both atmospheric and oceanic variables from the same set of GCMs
845 ensures consistency between the fisheries and marine ecosystems sector and other ISIMIP sectors. The
846 available variables in ISIMIP3b are interpolated from the native grids of the ocean models to a regular 1°
847 grid. This resolution is comparatively lower than that of the ISIMIP3a ocean input data due to the
848 generally reduced native resolution of CMIP6 GCM simulations compared to the ocean model used to
849 generate the oceanic forcings based on observational atmospheric forcings for ISIMIP3a.

850

851 **Table 8:** Oceanic climate-related forcing data provided within ISIMIP3b. Variables with suffixes -bot,
852 -surf, and -vint were obtained from the seafloor, the top layer of the ocean, and vertical integration,
853 respectively.

Variable	Variable specifier	Unit	Resolution	Datasets
----------	--------------------	------	------------	----------



Mass concentration of total phytoplankton expressed as chlorophyll	chl	kg m ⁻³	1° grid, vertically resolved, monthly	GFDL-ESM4, IPSL-CM6A-LR, MPI-ESM1-2-HR, UKESM1-0-LL
Sea floor depth	deptho	m	1° grid, constant	GFDL-ESM4, IPSL-CM6A-LR, MPI-ESM1-2-HR, UKESM1-0-LL
Downward flux of particulate organic carbon	expc-bot	mol m ⁻² s ⁻¹	1° grid, monthly	GFDL-ESM4, IPSL-CM6A-LR, MPI-ESM1-2-HR, UKESM1-0-LL
Particulate organic carbon content	intpoc	kg m ⁻²	1° grid, monthly	GFDL-ESM4, MPI-ESM1-2-HR, UKESM1-0-LL
Net primary organic carbon production by all types of phytoplankton	intpp	mol m ⁻² s ⁻¹	1° grid, monthly	GFDL-ESM4, IPSL-CM6A-LR, MPI-ESM1-2-HR, UKESM1-0-LL
Net primary organic carbon production by diatoms	intppdiat	mol m ⁻² s ⁻¹	1° grid, monthly	GFDL-ESM4, IPSL-CM6A-LR, UKESM1-0-LL
Net Primary Organic Carbon Production by Other Phytoplankton	intppmisc	mol m ⁻² s ⁻¹	1° grid, monthly	GFDL-ESM4, IPSL-CM6A-LR, UKESM1-0-LL
Net Primary Mole Productivity of Carbon by Picophytoplankton	intpppico	mol m ⁻² s ⁻¹	1° grid, monthly	GFDL-ESM4
Net Primary Organic Carbon Production of Carbon by Diazotrophs	intppdiaz	mol m ⁻² s ⁻¹	1° grid, monthly	GFDL-ESM4, MPI-ESM1-2-HR
Mixed layer depth defined by delta rho = 0.125	mlotstmax	m	1° grid, monthly	IPSL-CM6A-LR, MPI-ESM1-2-HR, UKESM1-0-LL
Dissolved oxygen concentration	o2, o2-bot, o2-surf	mol m ⁻³	1° grid, vertically resolved, ocean bottom and surface fields, monthly	GFDL-ESM4, IPSL-CM6A-LR, MPI-ESM1-2-HR, UKESM1-0-LL



pH	ph, ph-bot, ph-surf	1	1° grid, vertically resolved, ocean bottom and surface fields, monthly	GFDL-ESM4, IPSL-CM6A-LR, MPI-ESM1-2-HR, UKESM1-0-LL
Total phytoplankton carbon concentration	phyc, phyc-vint	mol m ⁻³	1° grid, vertically resolved and vertically integrated, monthly	GFDL-ESM4, IPSL-CM6A-LR, MPI-ESM1-2-HR, UKESM1-0-LL
Concentration of diatoms expressed as carbon in sea water	phydiat, phydiat-vint	mol m ⁻³	1° grid, vertically resolved and vertically integrated, monthly	GFDL-ESM4, IPSL-CM6A-LR, UKESM1-0-LL
Concentration of diazotrophs expressed as carbon in Sea Water	phydiaz, phydiaz-vint	mol m ⁻³	1° grid, vertically resolved and vertically integrated, monthly	GFDL-ESM4, MPI-ESM1-2-HR
Mole Content of Miscellaneous Phytoplankton Expressed as Carbon in Sea Water	phymisc, phymisc-vint	mol m ⁻²	1° grid, vertically resolved and vertically integrated, monthly	GFDL-ESM4, IPSL-CM6A-LR, MPI-ESM1-2-HR, UKESM1-0-LL
Mole Concentration of Picophytoplankton Expressed as Carbon in Sea Water	phypico, phypico-vint	mol m ⁻³	1° grid, vertically resolved and vertically integrated, monthly	GFDL-ESM4
Net Downward Shortwave Radiation at Sea Water Surface	rsndts	W m ⁻²	1° grid, monthly	GFDL-ESM4, IPSL-CM6A-LR, MPI-ESM1-2-HR
Sea Ice Area Fraction	siconc	%	1° grid, monthly	GFDL-ESM4, IPSL-CM6A-LR, MPI-ESM1-2-HR, UKESM1-0-LL



Sea water salinity	so, so-bot, so-surf	0.001	1° grid, vertically resolved, ocean bottom and surface fields, monthly	GFDL-ESM4, IPSL-CM6A-LR, MPI-ESM1-2-HR, UKESM1-0-LL
Sea water potential temperature	thetao	°C	1° grid, vertically resolved, monthly	GFDL-ESM4, IPSL-CM6A-LR, MPI-ESM1-2-HR, UKESM1-0-LL
Ocean model cell thickness	thkcello	m	1° grid, vertically resolved, monthly	GFDL-ESM4, IPSL-CM6A-LR, MPI-ESM1-2-HR, UKESM1-0-LL
Sea water potential temperature at sea floor (bottom)	tob	°C	1° grid, monthly	GFDL-ESM4, IPSL-CM6A-LR, MPI-ESM1-2-HR, UKESM1-0-LL
Sea surface temperature	tos	°C	1° grid, monthly	GFDL-ESM4, IPSL-CM6A-LR, MPI-ESM1-2-HR, UKESM1-0-LL
Sea water zonal velocity	uo	m s ⁻¹	1° grid, vertically resolved, monthly	IPSL-CM6A-LR, MPI-ESM1-2-HR, UKESM1-0-LL
Sea water meridional velocity	vo	m s ⁻¹	1° grid, vertically resolved, monthly	IPSL-CM6A-LR, MPI-ESM1-2-HR, UKESM1-0-LL
Concentration of mesozooplankton expressed as carbon in sea water	zmeso, zmeso-vint	mol m ⁻³	1° grid, vertically resolved and vertically integrated, monthly	GFDL-ESM4, IPSL-CM6A-LR, UKESM1-0-LL
Concentration of microzooplankton expressed as carbon in sea water	zmicro, zmicro-vint	mol m ⁻³	1° grid, vertically resolved and vertically integrated, monthly	GFDL-ESM4, IPSL-CM6A-LR, UKESM1-0-LL



Total Zooplankton Carbon Concentration	zooc, zooc-vint	mol m-3	1° grid, vertically resolved and vertically integrated, monthly	GFDL-ESM4, IPSL-CM6A-LR, MPI-ESM1-2-HR, UKESM1-0-LL
--	--------------------	---------	--	--

854

855 **2.4.2 Bias-adjusted global ocean forcings (‘de-biased’ sensitivity experiment)**

856 GCMs have been shown to have limitations in accurately representing various aspects of the present
857 climate system (Eyring et al., 2023), (Séférian et al., 2020), that are also expected to affect regional
858 physical and biogeochemical oceanic projections (Li et al., 2016), (Tagliabue et al., 2021). In particular,
859 biases in sea-surface temperature (SST, variable ‘tos’) and nutricline as well as thermocline depth
860 influence oceanic primary productivity, which in turn has major influence on various marine ecosystem
861 processes. Thus, reducing the substantial biases in GCMs’ ocean variables through bias-adjustment is
862 desirable. Typically, for bias-adjustment of atmospheric variables, statistical approaches are used where
863 a transfer function is trained to map the simulated historical distribution of the relevant variables to the
864 observed distribution and then applied to future simulations. Yet for oceanic variables, the scarcity of
865 comprehensive sub-surface observational data globally does not allow for a similar, direct adjustment of
866 the relevant variables. However, standalone ocean-biogeochemistry simulations, when driven by
867 observation-based atmospheric reanalysis data, have been demonstrated to considerably alleviate
868 SST-related biases and typically provide satisfactory simulations of the physical ocean and marine
869 biogeochemistry for the historical period (e.g. (Tsujino et al., 2020), (Barrier et al., 2023). Thus, an
870 alternative process-oriented bias-adjustment approach has been developed that relies on a
871 comprehensive ocean-biogeochemistry model that is forced by bias-adjusted atmospheric forcings. The
872 adjustment of the ISIMIP3b oceanic forcings builds on such a dynamical de-biasing approach (Lengaigne
873 et al., 2025), which relies on conducting forced oceanic simulations using the NEMO-PISCES
874 physical-biogeochemical ocean model (Madec, 2015), which is the oceanic component of the
875 IPSL-CM6A-LR climate model. The ocean model needs to be forced with high-frequency (3-hourly)
876 surface momentum, heat and freshwater fluxes. Since from the CMIP6 pre-industrial, historical, and
877 future scenario simulations used in ISIMIP3b these variables are only available at monthly resolution,
878 additional steps are necessary to generate climatological high-frequency fluxes first. In the following, we
879 first describe these preparatory steps, and then the de-biasing strategy, in more detail.

880

881 **High-frequency surface flux forcing.** Initially, a climatological simulation spanning the historical
882 period from 1958 to 2022 is performed by forcing the ocean model NEMO-PISCES with a single
883 repeating annual cycle representative of the 1990s’ climate conditions sourced from the “Repeat Year
884 Forcing” (RYF) from JRA55 reanalysis (Stewart et al., 2020). This simulation is driven using the CORE bulk
885 formulae (Large W. G., 2004), incorporating all surface atmospheric variables at 3-hourly resolution from
886 JRA55 RYF as inputs and storing 3-hourly momentum, heat and freshwater fluxes from this simulation.
887 These 3-hourly JRA55 RYF fluxes are the added to the monthly seasonal flux anomalies available from
888 the ISIMIP3b climate models for the pre-industrial (picontrol), historical (historical) and future SSP1-2.6
889 (ssp126), SSP3-7.0 (ssp370), and SSP5-8.5 (ssp585) scenarios. In this way, 3-hourly surface flux forcings



are created for all ISIMIP3b scenarios. Notably, this procedure results in sub-monthly variability mirroring that of the JRA55 RYF, rather than the variability simulated by the coupled climate model. This means that any projected changes in sub-monthly variability due to climate change are not integrated in the final de-biased product. However, to date, marine ecosystem modellers have not analysed sub-monthly variability anyways (and most marine ecosystem models are not suited to account for sub-monthly variability of forcings), making this approach suitable.

Alternatively, de-biased ocean simulations including GCM-based sub-monthly variability could be constructed by an alternative approach. In this scenario, 3-hourly surface atmospheric variables would be extracted directly from each GCM simulation, rather than from JRA55 RYF forced oceanic simulations. Forcing NEMO-PISCES with these variables using bulk formulae would once again produce the necessary 3-hourly surface fluxes, this time with variability consistent with the coupled GCM across all timescales. This approach however requires running a separate ocean simulation for each GCM and scenario to derive the surface fluxes, necessitating a much larger number of ocean model runs than the approach using JRA55 RYF. In addition, the 3-hourly input from the GCMs is not available without gaps.

De-biasing strategy. The 3-hourly surface fluxes, constructed as described above, then serve as forcings for another set of ocean model simulations. Notably, these simulations are not driven with bulk formulae but directly with surface fluxes to enable an online implementation of the surface heat flux feedbacks triggered by climate change into the forced ocean biogeochemistry model for historical and future simulations (Lengaigne et al., 2025). For bias-adjustment, the part of the anomalous surface fluxes that directly depends on climate change-induced SST warming is separated from the part that does not. Only the latter part is used as a direct flux input to the ocean model, while the former is implemented within NEMO-PISCES as an online relaxation to the warming signal from the debiased historical and future simulations using a spatially and seasonally variable feedback damping coefficient. This SST feedback coefficient, derived from observed surface variables, represents the Newtonian cooling negative feedback related to latent heat fluxes through the Clausius-Clapeyron relationship and the negative feedback related to upward long-wave radiation through Stefan's law (Zhang and Li 2014) and the positive downward longwave radiation feedback related to increasing temperature (Shakespeare et al. 2022). Application of this approach to the ocean model effectively reproduces the global SST changes simulated by CMIP6 models, as demonstrated in (Lengaigne et al., 2025).

In this way, physical and biogeochemical ocean simulations are generated for picontrl and historical climate forcings as well as for each of the future climate change scenarios, ensuring that the background climatological state is constrained by the reanalysis, while still accounting for both interannual and long-term climate variability simulated by the underlying GCM. Consequently, the resulting ocean-biogeochemistry simulations considerably mitigate the strong present-day climatological biases identified in the coupled models. Depending on data availability for the relevant monthly fluxes, this de-biasing procedure can be applied to any climate model.

Additionally, to generate observation-based oceanic forcings for ISIMIP3a, a reference simulation is also forced with the full JRA55 forcing (Tsujino et al. 2018) that includes observed inter-annual and decadal variability. This oceanic forcing is expected to be a valuable additional climate-related forcing for impact model evaluation within ISIMIP3a akin to the GFDL-MOM6-COBALT2 reanalysis-driven historical dataset



931 used in ISIMIP3a ((Frieler et al., 2024). The set of variables included in the de-biased dataset is a subset
932 to the one in the raw GCM dataset (Table 8), detailed in Table 9.

933

934 **Table 9:** Bias-adjusted ocean data to be used by global impact models in the ‘de-biased’ sensitivity
935 experiment in the fisheries and marine ecosystems sector

Variable	Variable specifier (variables in brackets are not directly available as model output but will have to be derived in post-processing)	Unit	Resolution	Forcing datasets
Mass concentration of total phytoplankton expressed as chlorophyll	chl	kg m ⁻³	1° grid, vertically resolved, monthly	JRA55+IPSL-CM6A-LR
Sea floor depth	deptho	m	1° grid, constant	JRA55+IPSL-CM6A-LR
Downward flux of particulate organic carbon	expc-bot	mol m ⁻² s ⁻¹	1° grid, monthly	JRA55+IPSL-CM6A-LR
Net primary organic carbon production by all types of phytoplankton	intpp	mol m ⁻² s ⁻¹	1° grid, monthly	JRA55+IPSL-CM6A-LR
Net primary organic carbon production by diatoms	intppdiat	mol m ⁻² s ⁻¹	1° grid, monthly	JRA55+IPSL-CM6A-LR
Net Primary Organic Carbon Production by Other Phytoplankton	intppmisc	mol m ⁻² s ⁻¹	1° grid, monthly	JRA55+IPSL-CM6A-LR
Mixed layer depth defined by delta rho = 0.125	mlotstmax	m	1° grid, monthly	JRA55+IPSL-CM6A-LR
Dissolved oxygen concentration	o2, (o2-bot), o2-surf	mol m ⁻³	1° grid, vertically resolved, ocean bottom and surface fields, monthly	JRA55+IPSL-CM6A-LR
pH	ph, (ph-bot), ph-surf	1	1° grid, vertically resolved, ocean	JRA55+IPSL-CM6A-LR



			bottom and surface fields, monthly	
Total phytoplankton carbon concentration	phyc, (phyc-vint)	mol m ⁻³	1° grid, vertically resolved and vertically integrated, monthly	JRA55+IPSL-CM6A-LR
Concentration of diatoms expressed as carbon in sea water	phydiat, (phydiat-vint)	mol m ⁻³	1° grid, vertically resolved and vertically integrated, monthly	JRA55+IPSL-CM6A-LR
Mole Content of Miscellaneous Phytoplankton Expressed as Carbon in Sea Water	phymisc, (phymisc-vint)	mol m ⁻²	1° grid, vertically resolved and vertically integrated, monthly	JRA55+IPSL-CM6A-LR
Net Downward Shortwave Radiation at Sea Water Surface	rsndts	W m ⁻²	1° grid, monthly	JRA55+IPSL-CM6A-LR
Sea water salinity	so, (so-bot), so-surf	0.001	1° grid, vertically resolved, ocean bottom and surface fields, monthly	JRA55+IPSL-CM6A-LR
Sea water potential temperature	thetao	°C	1° grid, vertically resolved, monthly	JRA55+IPSL-CM6A-LR
Ocean model cell thickness	thkcello	m	1° grid, vertically resolved, monthly	JRA55+IPSL-CM6A-LR
Sea water potential temperature at sea floor (bottom)	(tob)	°C	1° grid, monthly	JRA55+IPSL-CM6A-LR
Sea surface temperature	tos	°C	1° grid, monthly	JRA55+IPSL-CM6A-LR
Sea water zonal velocity	uo	m s ⁻¹	1° grid, vertically resolved, monthly	JRA55+IPSL-CM6A-LR
Sea water meridional velocity	vo	m s ⁻¹	1° grid, vertically resolved, monthly	JRA55+IPSL-CM6A-LR
Concentration of mesozooplankton	zmeso, (zmeso-vint)	mol m ⁻³	1° grid, vertically resolved and vertically integrated	JRA55+IPSL-CM6A-LR



expressed as carbon in sea water			integrated, monthly	
Concentration of microzooplankton expressed as carbon in sea water	zmicro, (zmicro-vint)	mol m ⁻³	1° grid, vertically resolved and vertically integrated, monthly	JRA55+IPSL-CM6A-LR
Total Zooplankton Carbon Concentration	zooc, (zooc-vint)	mol m ⁻³	1° grid, vertically resolved and vertically integrated, monthly	JRA55+IPSL-CM6A-LR

936

937 2.4.3 Bias-adjusted regional ocean forcings ('de-biased' sensitivity experiment)

938 Regional marine ecosystem models are most often calibrated to reproduce observed environmental
939 variables when driven by observed sea surface and bottom temperature, primary production
940 (phytoplankton production), and zooplankton biomass. However, that would still lead to biases in the
941 historical simulations if the impact model was forced by biased simulated input data instead of
942 observational data. To reduce this effect the GCM-based input data has been adjusted such that the
943 historical GCM simulations match observational data for certain regions (Eddy et al., 2025). The
944 adjustment is based on the delta approach where simulated and observational forcing data X_{sim} and X_{obs}
945 are averaged across a given historical reference period to determine the bias $\Delta = \text{mean}(X_{sim}) - \text{mean}$
946 (X_{obs}) that is then subtracted from the simulated forcing data. This method preserves the trend in the
947 forcing data and its internal variability. Some ocean forcing variables are not an exact match with
948 variables used in regional marine ecosystem models. For example, sea water potential temperature
949 (thetao), concentration of diatoms (phydiat-vint), or concentration of mesozooplankton (zmeso-vint)
950 may first be converted to other indicators that are then used as input for the regional marine ecosystem
951 models. In these cases the derived indicator is corrected using the delta method (see Table 10).

952 **Table 10:** Bias-adjusted ocean data to be used by regional impact models in the 'de-biased' sensitivity
953 experiment in the fisheries and marine ecosystems sector

Variable	Variable specifier	Unit	Resolution	Forcing datasets
Southern Benguela Current				
Net primary organic carbon production by all types of phytoplankton	intpp	mol m ⁻² s ⁻¹	1° grid, monthly	Corrected based on observed primary production for the southern Benguela current based on the delta method where the adjustment target is data from 1978 for the EwE model and 1990 for the Atlantis model



Sea water potential temperature	thetao	°C	1° grid, vertically resolved, monthly	Raw GCM temperature data converted to temperatures at 0-50, 50-100, 100-300 and 300-500 m according to the configuration for the southern Benguela Atlantis model, and 0-50 and 300-500 m for the EwE model.
Cook Strait				
Net primary organic carbon production by all types of phytoplankton	intpp	mol m ⁻² s ⁻¹	1° grid, monthly	Corrected based on observed primary production for Cook Strait using the delta method where observational target data is from 1950
East Bass Strait				
Net primary organic carbon production by all types of phytoplankton	intpp	mol m ⁻² s ⁻¹	1° grid, monthly	Corrected based on observed primary production for East Bass Strait using the delta method where observational target data is from 1994
East Bering Sea				
Concentration of diatoms expressed as carbon in sea water	phydiat-vint	mol m ⁻³	1/4° grid, vertically resolved and vertically integrated, monthly	Converted to phytoplankton size classes used in East Bering Sea mizer model then corrected using the delta method for the period 1982–1993
Concentration of diazotrophs expressed as carbon in sea water	phydiaz-vint	mol m ⁻³	1/4° grid, vertically resolved and vertically integrated, monthly	Converted to phytoplankton size classes used in East Bering Sea mizer model then corrected using the delta method for the period 1982–1993
Concentration of picoplankton expressed as carbon in sea water	phypico-vint	mol m ⁻³	1/4° grid, vertically resolved and vertically integrated, monthly	Converted to phytoplankton size classes used in East Bering Sea mizer model then corrected using the delta method for the period 1982–1993
Concentration of mesozooplankton expressed as carbon in sea water	zmeso-vint	mol m ⁻³	1/4° grid, vertically resolved and vertically integrated, monthly	Converted to zooplankton size classes used in East Bering Sea mizer model then corrected using the delta method for the period 1982–1993



Concentration of microzooplankton expressed as carbon in sea water	zmicro-vint	mol m-3	1/4° grid, vertically resolved and vertically integrated, monthly	Converted to zooplankton size classes used in East Bering Sea mizer model then corrected using the delta method for the period 1982-1993
Sea surface temperature	tos	°C	1/4° grid, monthly	Corrected based on configuration for the East Bering Sea mizer model using the delta method for the period 1982–1993
Hawai'i				
Concentration of diatoms expressed as carbon in sea water	phydiat-vint	mol m-3	1/4° grid, vertically resolved and vertically integrated, monthly	Converted to phytoplankton size classes used in Hawaii mizer model (Woodworth-Jefcoats, 2022) then corrected using the delta method
Concentration of diazotrophs expressed as carbon in sea water	phydiaz-vint	mol m-3	1/4° grid, vertically resolved and vertically integrated, monthly	Converted to phytoplankton size classes used in Hawaii mizer model then corrected using the delta method
Concentration of picoplankton expressed as carbon in sea water	phypico-vint	mol m-3	1/4° grid, vertically resolved and vertically integrated, monthly	Converted to phytoplankton size classes used in Hawaii mizer model then corrected using the delta method
Concentration of mesozooplankton expressed as carbon in sea water	zmeso-vint	mol m-3	1/4° grid, vertically resolved and vertically integrated, monthly	Converted to zooplankton size classes used in Hawaii mizer model then corrected using the delta method
Concentration of microzooplankton expressed as carbon in sea water	zmicro-vint	mol m-3	1/4° grid, vertically resolved and vertically integrated, monthly	Converted to zooplankton size classes used in Hawaii mizer model then corrected using the delta method
Sea water potential temperature	thetao	°C	1/4° grid, vertically resolved, monthly	Converted to temperature used in Hawaii Mizer model then corrected based on observed sea water potential temperature for Hawaii using the delta method from



				1961–1980 with observed temperature data from the World Ocean Atlas
--	--	--	--	---

954

955

956 **2.5 Future Lightning Data**

957 For the ‘varlightning’ sensitivity experiment we provide temporally varying lightning density (strokes km⁻²
958 day⁻¹) for the period 2015-2100 on monthly resolution (monthly mean of daily lightning stroke density)
959 and the standard 0.5° global grid. This dataset may be used in a range of applications, for example, to
960 understand the influence of lightning on wildfire ignition or atmospheric composition.

961 The lightning density is derived from future climate simulations by UKESM1-0-LL and an empirical
962 relationship between Convective Available Potential Energy (CAPE) and lightning strokes based on the
963 WWLLN Global Lightning Climatology and time-series (WGLC) (Kaplan & Lau, 2021, 2022). Daily mean
964 CAPE is calculated from non bias-adjusted air temperature, air pressure, and specific humidity on
965 pressure levels from the surface to the top of the troposphere.

966 The relationship between daily CAPE and daily lightning is estimated by linear regression of
967 log-transformed CAPE derived from the GCM-calculated CAPE during the period of overlapping model
968 output and observed daily lightning from WGLC (2015-2020) for each gridcell and month of the year.
969 Where <10 observations of daily lightning were available over the calibration period, we used global
970 mean regression parameters.

971 The empirical relationships are applied to the daily CAPE data from the UKESM1-0-LL simulations for all
972 three climate scenarios SSP1-2.6, SSP3-7.0, and SSP5-8.5. The associated lightning densities were
973 monthly averaged. To maintain the spatial structure of lightning observed at present, lightning
974 anomalies compared to the simulated 2015-2020 climatological reference were added to the observed
975 present-day lightning climatology from WGLC for 2015-2020. The ‘varlightning’ sensitivity experiment is
976 assumed to start from the default historical group I simulation, assuming the Flash Rate Monthly
977 Climatology (Cecil, 2006), not changing with climate change.

978

979

980 **Table 11:** Future lightning forcing data provided within ISIMIP3b.

Variable	Variable specifier	Unit	Resolution	Datasets
Monthly flash rate	lightning	km-2 d-1	0.5° grid, monthly	Derived from UKESM1-0-LL (SSP1-2.6, SSP3-7.0, and SSP5-8.5) using an empirical relationship between Convective Available



				Potential Energy (CAPE) and lightning densities (Kaplan et al., 2023).
--	--	--	--	--

981
982
983

984 **3 Conclusions**

985

986 This paper gives an overview over the ISIMIP3b, group I and II experiments and the provided
987 climate-related forcing data sets. The simulations assuming fixed 2015 direct human forcings and a low
988 (ssp126) and two high emission scenarios (ssp370 and ssp585) are designed to describe the impacts of
989 different levels of climate change on present day natural and human systems. The set-up allows e.g. for
990 testing to what degree the (bio-)physical impacts scale with global mean temperature change and could
991 therefore be translated to other global warming pathways than the ones considered here. While a
992 functional relationship between the considered impact indicator and global mean temperature change
993 (or other climate variables) could be trained on ssp585 simulations because of the high warming levels
994 reached, its performance could then be tested on ssp370 and ssp126. However, in such a setting it has
995 to be taken into account that ssp370 is different from the other scenarios with regard to particularly
996 high aerosol emissions and high decreases in forest areas going beyond the assumptions in the other
997 models. So it has been shown that the increase of global mean precipitation with global warming is
998 much weaker in SSP3-7.0 than in the other scenarios (Shiogama et al., 2023).

999

1000 This paper is intended to work as a catalogue where the climate impact modellers can find all relevant
1001 information about the climate-related forcings needed as reference for the impact model simulations
1002 generated within the CMIP6-based ISIMIP3b, group I (historical period) and group II (future projections).
1003 As a continuous process we would like to improve or complement these data sets wherever possible. So
1004 this paper can also be read as a call to either contribute by additional input data that allows other
1005 sectors to join the current simulation round or by methods that could be used to generate additional
1006 data sets for the next simulation round that will likely build on CMIP7 simulations. The following
1007 climate-related forcings have been identified as still missing and particularly critical to be added to a
1008 fourth simulation round of ISIMIP: i) temporally resolved lightning data accounting for changes in
1009 climate, ii) bias-adjusted oceanic forcing data, iii) projected coastal water levels in high temporal
1010 resolution accounting for extremes and representing the effects of long term sea level rise in line with
1011 the underlying global climate simulations, and v) ozone concentration fields in line with the GCM
1012 simulations. While a bias-adjustment of the oceanic forcings is already suggested in section 2.4.2, the
1013 approach does not preserve the daily variability of the raw oceanic forcings as it requires atmospheric
1014 surface flux only available in monthly resolution from the ISIMIP3b GCMs. To ensure the consistency on
1015 daily time scale, we have submitted an associated request for CMIP7 whose simulations will be used
1016 within the next round of ISIMIP. The generation of high resolution coastal water levels is ongoing
1017 research described in section 2.2.3. In particular the generation of the short term variability that will
1018 have to be added to the long term trends in water levels still has to be developed and prove to fulfill the
1019 demands. In addition, it would be great to also provide estimates of the extreme coastal water levels
1020 associated with the tropical cyclone tracks and wind fields we provide within ISIMIP3b (see section 2.2).



1021 There is a general demand for higher resolution climate-related forcings including both, the oceanic and
1022 the atmospheric components ideally accounting for heat island effects. As the ISIMIP climate-related
1023 forcings have to be globally consistent in the sense that they have to represent the daily variability of
1024 the underlying coarse resolution GCMs, we cannot use data from dynamical downscaling approaches
1025 using boundary conditions from different GCM runs as for example available through CORDEX. However,
1026 it seems to be appealing to harmonize the selection of the ISIMIP GCMs with a priority setting regarding
1027 the GCM-based boundary conditions within CORDEX.

1028

1029 The climate-related forcings described here are also provided as input for the new ISIMIP3b, group III
1030 simulations where the associated Direct Human Forcings (DHF) are not held constant at 2015 levels but
1031 are projected into the future in line with i) the population growth and economic development
1032 associated with the considered Shared Socioeconomic Pathways (SSPs) and mitigation measures
1033 required to reach the prescribed levels of climate forcings associated with the climate projections ('no
1034 adaptation' experiments) and ii) additionally accounting for the impacts of climate change ('adaptation'
1035 experiments). The collection of the associated DHF will be described in a separate paper.

1036

1037 **Code and data availability.** The MIT data on tropical cyclone tracks with wind and precipitation fields
1038 data shall be used for non-commercial research or academic purposes only. Data can be made available
1039 by the ISIMIP team upon written consent by Kerry Emanuel (MIT, email: emanuel@mit.edu).

1040 All other input data described are available for participating modelers with a respective account from
1041 the DKRZ server. Data will be made publicly available, and most data are already publicly available at the
1042 ISIMIP data repository at <https://data.isimip.org/> (ISIMIP data repository, 2025) and availability is
1043 documented in the ISIMIP Input data table
1044 <https://www.isimip.org/gettingstarted/input-data-bias-adjustment/> (ISIMIP input data table, 2025)
1045 where the way to access the data is described as well. Model output is already partly available
1046 <https://data.isimip.org/> (ISIMIP data repository, 2025). The ISIMIP repository fulfills the archive
1047 standards as stated in the "GMD code and data policy". The repository is hosted and maintained by the
1048 Potsdam Institute for Climate Impact Research (PIK). Data can only be published or removed from the
1049 repository by the ISIMIP data team, which is monitored by the ISIMIP steering committee according to
1050 the organizational structure of ISIMIP. DOIs are used to refer to datasets in a persistent way. Whenever a
1051 dataset is replaced for any reason a copy is kept on tape, and a new DOI is issued, while the old DOI is
1052 kept online with information on how to retrieve the archived data. Detailed information can be found in
1053 the ISIMIP terms of use at <https://www.isimip.org/gettingstarted/terms-of-use/> (ISIMIP terms of use,
1054 2023).

1055

1056 **Author contributions**

1057 KF lead the project and developed the concept with contributions from JS, MM, CO, CPOR, SH, JLB, CSH,
1058 CMP, TDE, KOC, CN, RH, DPT, OM, SJC, JJ, SR, GL, SC, EB, AGS, NS, JC, SH, CB, AG, FL, SNG, HMS, FH, TH,
1059 RM, DP, WT, DMB, RL, AIA, MF, MB, RR, and IDG. JV, MB, JK, IDVDV, LN, IJS supported the quality control
1060 and curation of the climate-related forcing data and the protocol development together with the
1061 sectoral ISIMIP coordinators listed as co-authors. SL developed the method and generated the
1062 downscaled and bias-adjusted atmospheric climate forcing data. MM and ST provided the description of



the approach to generate the coastal water level data. ML provided the description of the method to bias-adjust the global oceanic forcings. TV, DQC, CYL, SJC, and KE provided TC data. JOK and AK provided the future lightning data. KF prepared the manuscript with contributions from all co-authors.

Competing interests

At least one of the (co-)authors is a member of the editorial board of GMD

Acknowledgements

This article is based upon work from COST Action CA19139 PROCLIAS (PROcess-based models for Climate Impact Attribution across Sectors), supported by COST (European Cooperation in Science and Technology; <https://www.cost.eu>). SL received funding from the German Research Foundation (DFG, project number 427397136). MB acknowledges funding from the BELSPO STEREO IV project SR/00/414. SC, AGS, MB and NS acknowledge funding through NERC NE/V01854X/1 (MOTHERSHIP). This research has received funding from the German Federal Ministry of Education and Research (BMBF) under the research projects QUIDIC (grant agreement no. 01LP1907A) and ISI-Access (16QK05), from the Horizon 2020 Framework Programme of the European Union under the projects RECEIPT (grant agreement no. 820712). C.-Y. L is supported by Palisades Geophysical Institute (PGI) Young Scientist Award. KOC acknowledges support from the National Research Foundation of South Africa (grant 136481) and the resources from the Cluster for High Performance Computing-CSIR. FL is supported by the National Key Research and Development Program of China (2022YFE0106500). DPT acknowledges funding from the Jarislowsky Foundation and NSERC. IDG acknowledges funding of the European Research Council (ERC Starting Grant, GROW-101041110).



1089 References

1090

- 1091 Adler, R. F., Huffman, G. J., Chang, A., Ferraro, R., Xie, P.-P., Janowiak, J., Rudolf, B., Schneider, U., Curtis,
1092 S., Bolvin, D., Gruber, A., Susskind, J., Arkin, P., & Nelkin, E. (2003). The Version-2 Global
1093 Precipitation Climatology Project (GPCP) Monthly Precipitation Analysis (1979–Present). *Journal of*
1094 *Hydrometeorology*, 4(6), 1147–1167.
1095 [https://doi.org/10.1175/1525-7541\(2003\)004<1147:TVGPCP>2.0.CO;2](https://doi.org/10.1175/1525-7541(2003)004<1147:TVGPCP>2.0.CO;2)
- 1096 Andela, B., Broetz, B., de Mora, L., Drost, N., Eyring, V., Koldunov, N., Lauer, A., Mueller, B., Predoi, V.,
1097 Righi, M., Schlund, M., Vegas-Regidor, J., Zimmermann, K., Adeniyi, K., Arnone, E., Bellprat, O., Berg,
1098 P., Bock, L., Caron, L.-P., ... Weigel, K. (2020). *ESMValTool*. <https://doi.org/10.5281/zenodo.3970975>
- 1099 Andela, B., Broetz, B., de Mora, L., Drost, N., Eyring, V., Koldunov, N., Lauer, A., Predoi, V., Righi, M.,
1100 Schlund, M., Vegas-Regidor, J., Zimmermann, K., Bock, L., Diblen, F., Dreyer, L., Earnshaw, P., Hassler,
1101 B., Little, B., & Loosveldt-Tomas, S. (2020). *ESMValCore*. <https://doi.org/10.5281/zenodo.3952695>
- 1102 Barrier, N., Lengaigne, M., Rault, J., Person, R., Ethé, C., Aumont, O., & Maury, O. (2023). Mechanisms
1103 underlying the epipelagic ecosystem response to ENSO in the equatorial Pacific ocean. *Progress in*
1104 *Oceanography*, 213, 103002. <https://doi.org/10.1016/j.pocean.2023.103002>
- 1105 Bock, L., Lauer, A., Schlund, M., Barreiro, M., Bellouin, N., Jones, C., Meehl, G. A., Predoi, V., Roberts, M.
1106 J., & Eyring, V. (2020). Quantifying progress across different CMIP phases with the ESMValTool.
1107 *Journal of Geophysical Research*, 125(21). <https://doi.org/10.1029/2019jd032321>
- 1108 Boucher, O., Denvil, S., Levavasseur, G., Cozic, A., Caubel, A., Foujols, M.-A., Meurdesoif, Y., Cadule, P.,
1109 Devilliers, M., Dupont, E., & Lurton, T. (2019). *IPSL IPSL-CM6A-LR model output prepared for CMIP6*
1110 *ScenarioMIP* [Dataset]. Earth System Grid Federation. <https://doi.org/10.22033/ESGF/CMIP6.1532>
- 1111 Boucher, O., Denvil, S., Levavasseur, G., Cozic, A., Caubel, A., Foujols, M.-A., Meurdesoif, Y., Cadule, P.,
1112 Devilliers, M., Ghattas, J., Lebas, N., Lurton, T., Mellul, L., Musat, I., Mignot, J., & Cheruy, F. (2018).



- 1113 *IPSL IPSL-CM6A-LR model output prepared for CMIP6 CMIP* [Dataset]. Earth System Grid Federation.
- 1114 <https://doi.org/10.22033/ESGF/CMIP6.1534>
- 1115 Boucher, O., Servonnat, J., Albright, A. L., Aumont, O., Balkanski, Y., Bastrikov, V., Bekki, S., Bonnet, R.,
- 1116 Bony, S., Bopp, L., Braconnot, P., Brockmann, P., Cadule, P., Caubel, A., Cheruy, F., Codron, F., Cozic,
- 1117 A., Cugnet, D., D'Andrea, F., ... Vuichard, N. (2020). Presentation and evaluation of the
- 1118 IPSL-CM6A-LR climate model. *Journal of Advances in Modeling Earth Systems*, 12(7).
- 1119 <https://doi.org/10.1029/2019ms002010>
- 1120 Büchner, M., & Reyer, C. (2022). *ISIMIP3b atmospheric composition input data* [Dataset]. ISIMIP
- 1121 Repository. <https://doi.org/10.48364/ISIMIP.482153.1>
- 1122 Buck, A. L. (1981). New Equations for Computing Vapor Pressure and Enhancement Factor. *Journal of*
- 1123 *Applied Meteorology and Climatology*, 20(12), 1527–1532.
- 1124 [https://doi.org/10.1175/1520-0450\(1981\)020<1527:NEFCVP>2.0.CO;2](https://doi.org/10.1175/1520-0450(1981)020<1527:NEFCVP>2.0.CO;2)
- 1125 Camargo, S. J., Tippett, M. K., Sobel, A. H., Vecchi, G. A., & Zhao, M. (2014). Testing the Performance of
- 1126 Tropical Cyclone Genesis Indices in Future Climates Using the HiRAM Model. *Journal of Climate*,
- 1127 27(24), 9171–9196. <https://doi.org/10.1175/JCLI-D-13-00505.1>
- 1128 Cannon, A. J. (2018). Multivariate quantile mapping bias correction: an N-dimensional probability
- 1129 density function transform for climate model simulations of multiple variables. *Climate Dynamics*,
- 1130 50(1), 31–49. <https://doi.org/10.1007/s00382-017-3580-6>
- 1131 Cecil, D. (2006). *LIS/OTD 0.5 Degree High Resolution Monthly Climatology (HRMC)* [Dataset]. NASA
- 1132 Global Hydrometeorology Resource Center DAAC. <https://doi.org/10.5067/LIS/LIS-OTD/DATA303>
- 1133 Cucchi, M., Weedon, G. P., Amici, A., Bellouin, N., Lange, S., Müller Schmied, H., Hersbach, H., &
- 1134 Buontempo, C. (2020). WFDE5: bias-adjusted ERA5 reanalysis data for impact studies. *Earth System*
- 1135 *Science Data*, 12(3), 2097–2120. <https://doi.org/10.5194/essd-12-2097-2020>
- 1136 Dunne, J. P., Horowitz, L. W., Adcroft, A. J., Ginoux, P., Held, I. M., John, J. G., Krasting, J. P., Malyshev, S.,



- 1137 Naik, V., Paulot, F., Shevliakova, E., Stock, C. A., Zadeh, N., Balaji, V., Blanton, C., Dunne, K. A.,
1138 Dupuis, C., Durachta, J., Dussin, R., ... Zhao, M. (2020). The GFDL earth system model version 4.1
1139 (GFDL-ESM 4.1): Overall coupled model description and simulation characteristics. *Journal of*
1140 *Advances in Modeling Earth Systems*, 12(11). <https://doi.org/10.1029/2019ms002015>
- 1141 Durack, P. J. (n.d.). *CMIP6 source_id values*. Retrieved January 16, 2023, from
1142 https://wcrp-cmip.github.io/CMIP6_CVs/docs/CMIP6_source_id.html
- 1143 Eddy, T. D., Heneghan, R. F., Bryndum-Buchholz, A., Fulton, E. A., Harrison, C. S., Tittensor, D. P., Lotze, H.
1144 K., Ortega-Cisneros, K., Novaglio, C., Bianchi, D., Büchner, M., Bulman, C., Cheung, W. W. L.,
1145 Christensen, V., Coll, M., Everett, J. D., Fierro-Arcos, D., Galbraith, E. D., Gascuel, D., ... Blanchard, J.
1146 L. (2025). Global and regional marine ecosystem models reveal key uncertainties in climate change
1147 projections. *Earth's Future*, 13(3). <https://doi.org/10.1029/2024ef005537>
- 1148 Emanuel, K., DesAutels, C., Holloway, C., & Korty, R. (2004). Environmental Control of Tropical Cyclone
1149 Intensity. *Journal of the Atmospheric Sciences*, 61(7), 843–858.
1150 [https://doi.org/10.1175/1520-0469\(2004\)061<0843:ECOTCI>2.0.CO;2](https://doi.org/10.1175/1520-0469(2004)061<0843:ECOTCI>2.0.CO;2)
- 1151 Emanuel, K., Sundararajan, R., & Williams, J. (2008). Hurricanes and Global Warming: Results from
1152 Downscaling IPCC AR4 Simulations. *Bulletin of the American Meteorological Society*, 89(3),
1153 347–368. <https://doi.org/10.1175/BAMS-89-3-347>
- 1154 Eyring, V., Bony, S., Meehl, G. A., Senior, C. A., Stevens, B., Stouffer, R. J., & Taylor, K. E. (2016). Overview
1155 of the Coupled Model Intercomparison Project Phase 6 (CMIP6) experimental design and
1156 organization. *Geoscientific Model Development*, 9(5), 1937–1958.
1157 <https://doi.org/10.5194/gmd-9-1937-2016>
- 1158 Eyring, V., Gillett, N. P., Achuta Rao, K. M., Barimalala, R., Barreiro Parrillo, M., Bellouin, N., V.
1159 Masson-Delmotte, P. Zhai, A. Pirani, S. L. Connors, C. Péan, S. Berger, & Intergovernmental Panel on
1160 Climate Change (IPCC). (2023). Human Influence on the Climate System. In *Climate Change 2021 –*



- 1161 *The Physical Science Basis: Working Group I Contribution to the Sixth Assessment Report of the*
1162 *Intergovernmental Panel on Climate Change* (pp. 423–552). Cambridge University Press.
1163 <https://doi.org/10.1017/9781009157896.005>
- 1164 Fosu, B., Sobel, A., Camargo, S., Tippett, M., Hemmati, M., Bowen, S., & Bloemendaal, N. (2024).
1165 Assessing future tropical cyclone risk using downscaled 1 CMIP6 projections. *Journal of Catastrophe*
1166 *Risk and Resilience*, 2(1). <https://doi.org/10.63024/dpva-2pa1>
- 1167 Frieler, K. (submitted 2023). Scenario Set-up and the new CMIP6-based climate-related forcings
1168 provided within the third round of the Inter-Sectoral Model Intercomparison Project (ISIMIP3b,
1169 group I and II). *Geoscientific Model Development*.
- 1170 Frieler, K., Lange, S., Piontek, F., Reyer, C. P. O., Schewe, J., Warszawski, L., Zhao, F., Chini, L., Denvil, S.,
1171 Emanuel, K., Geiger, T., Halladay, K., Hurtt, G., Mengel, M., Murakami, D., Ostberg, S., Popp, A., Riva,
1172 R., Stevanovic, M., ... Yamagata, Y. (2017). Assessing the impacts of 1.5 °C global warming –
1173 simulation protocol of the Inter-Sectoral Impact Model Intercomparison Project (ISIMIP2b).
1174 *Geoscientific Model Development*, 10(12), 4321–4345. <https://doi.org/10.5194/gmd-10-4321-2017>
- 1175 Frieler, K., Volkholz, J., Lange, S., Schewe, J., Mengel, M., del Rocio Rivas López, M., Otto, C., Reyer, C. P.
1176 O., Karger, D. N., & del Valle Gitta Lasslop Sarah Chadburn Eleanor Burke Angela Gallego-Sala Noah
1177 Smith Jinfeng Chang Stijn Hantson Chantelle Burton Anne Gädeke Fang Li Simon N. Gosling Hannes
1178 Müller Schmied Fred Hattermann Jida Wang Fangfang Yao Thomas Hickler Rafael Marcé Don
1179 Pierson Wim Thiery Daniel Mercado-Bettín Robert Ladwig Ana Isabel Ayala-Zamora Matthew
1180 Forrest and Michel Bechtold, J. T. M. S. T. C. M. J. L. B. C. S. H. C. M. P. T. D. E. K. O.-C. C. N. Y. R. R. A.
1181 W. C. S. X. L. R. H. D. T. O. M. M. B. T. V. T. W. F. S. I. J. S. J. K. I. V. J. J. C. M. S. R. J. K. I. D. V. (2024,
1182 January 4). *Scenario setup and forcing data for impact model evaluation and impact attribution*
1183 *within the third round of the Inter-Sectoral Model Intercomparison Project (ISIMIP3a)*. *Geoscientific*
1184 *Model Development*.



- 1185 [https://www.google.com/url?q=https://doi.org/10.5194/gmd-17-1-2024&sa=D&source=docs&ust=](https://www.google.com/url?q=https://doi.org/10.5194/gmd-17-1-2024&sa=D&source=docs&ust=1704377607845951&usg=AOvVaw3hFVXAV75ZSOClc8itQfEs)
- 1186 [1704377607845951&usg=AOvVaw3hFVXAV75ZSOClc8itQfEs](https://www.google.com/url?q=https://doi.org/10.5194/gmd-17-1-2024&sa=D&source=docs&ust=1704377607845951&usg=AOvVaw3hFVXAV75ZSOClc8itQfEs)
- 1187 (Frieler, K.,) Volkholz, J., Lange, S., Schewe, J., Mengel, M., del Rocío Rivas López, M., Otto, C., Reyer, C.
- 1188 P. O., Karger, D. N., Malle, J. T., Treu, S., Menz, C., Blanchard, J. L., Harrison, C. S., Petrik, C. M., Eddy,
- 1189 T. D., Ortega-Cisneros, K., Novaglio, C., Rousseau, Y., ... Bechtold, M. (2024). Scenario setup and
- 1190 forcing data for impact model evaluation and impact attribution within the third round of the
- 1191 Inter-Sectoral Impact Model Intercomparison Project (ISIMIP3a). *Geoscientific Model Development*,
- 1192 17(1), 1–51. <https://doi.org/10.5194/gmd-17-1-2024>
- 1193 Frieler, K., Volkholz, J., Lange, S., Schewe, J., Mengel, M., Rivas López, M. del R., Otto, C., Reyer, C. P. O.,
- 1194 Karger, D. N., Malle, J. T., Treu, S., Menz, C., Blanchard, J. L., Harrison, C. S., Petrik, C. M., Eddy, T. D.,
- 1195 Ortega-Cisneros, K., Novaglio, C., Rousseau, Y., ... Bechtold, M. (2023). Scenario set-up and forcing
- 1196 data for impact model evaluation and impact attribution within the third round of the
- 1197 Inter-Sectoral Model Intercomparison Project (ISIMIP3a). In *EGUsphere*.
- 1198 <https://doi.org/10.5194/egusphere-2023-281>
- 1199 Geiger, T., Gütschow, J., Bresch, D. N., Emanuel, K., & Frieler, K. (2021). Double benefit of limiting global
- 1200 warming for tropical cyclone exposure. *Nature Climate Change*, 11(10), 861–866.
- 1201 <https://doi.org/10.1038/s41558-021-01157-9>
- 1202 Gennaretti, F., Sangelantoni, L., & Grenier, P. (2015). Toward daily climate scenarios for Canadian Arctic
- 1203 coastal zones with more realistic temperature-precipitation interdependence. *JGR: Atmospheres*,
- 1204 120(23), 11,862–11,877. <https://doi.org/10.1002/2015JD023890>
- 1205 Gillett, N. P., Shiogama, H., Funke, B., Hegerl, G., Knutti, R., Matthes, K., Santer, B. D., Stone, D., &
- 1206 Tebaldi, C. (2016). The detection and Attribution Model Intercomparison Project (DAMIP v1.0)
- 1207 contribution to CMIP6. *Geoscientific Model Development*, 9(10), 3685–3697.
- 1208 <https://doi.org/10.5194/gmd-9-3685-2016>



- 1209 Good, P., Sellar, A., Tang, Y., Rumbold, S., Ellis, R., Kelley, D., Kuhlbrodt, T., & Walton, J. (2019). *MOHC*
- 1210 *UKESM1.0-LL model output prepared for CMIP6 ScenarioMIP* [Dataset]. Earth System Grid
- 1211 Federation. <https://doi.org/10.22033/ESGF/CMIP6.1567>
- 1212 Grenier, P. (2018). Two Types of Physical Inconsistency to Avoid with Univariate Quantile Mapping: A
- 1213 Case Study over North America Concerning Relative Humidity and Its Parent Variables. *Journal of*
- 1214 *Applied Meteorology and Climatology*, 57(2), 347–364. <https://doi.org/10.1175/JAMC-D-17-0177.1>
- 1215 Haerter, J. O., Hagemann, S., Moseley, C., & Piani, C. (2011). Climate model bias correction and the role
- 1216 of timescales. *Hydrology and Earth System Sciences*, 15(3), 1065–1079.
- 1217 <https://doi.org/10.5194/hess-15-1065-2011>
- 1218 Hausfather, Z., & Peters, G. P. (2020, January 29). *Emissions – the “business as usual” story is misleading*.
- 1219 Nature Publishing Group UK. <https://doi.org/10.1038/d41586-020-00177-3>
- 1220 Hersbach, H., Bell, B., Berrisford, P., Hirahara, S., Horányi, A., Muñoz-Sabater, J., Nicolas, J., Peubey, C.,
- 1221 Radu, R., Schepers, D., Simmons, A., Soci, C., Abdalla, S., Abellan, X., Balsamo, G., Bechtold, P.,
- 1222 Biavati, G., Bidlot, J., Bonavita, M., ... Jean-Noël Thépaut. (2020). The ERA5 global reanalysis.
- 1223 *Quarterly Journal of the Royal Meteorological Society*, 146(730), 1999–2049.
- 1224 <https://doi.org/10.1002/qj.3803>
- 1225 Holland. (1980). An Analytic Model of the Wind and Pressure Profiles in Hurricanes, Mon. *Mon. Weather*
- 1226 *Rev*, 108, 1212–1218.
- 1227 Holland. (2008). A revised hurricane pressure–wind model. *Monthly Weather Review*, 136(9),
- 1228 3432–3445. <https://doi.org/10.1175/2008mwr2395.1>
- 1229 *ISIMIP3b simulation protocol*. (2023). <https://protocol.isimip.org/>
- 1230 ISIMIP data repository: ISIMIP [data set], <https://data.isimip.org/>, last access: 28 April 2025.
- 1231 ISIMIP Input data table: ISIMIP [data set],
- 1232 <https://www.isimip.org/gettingstarted/input-data-bias-adjustment/>, last access: 28 April 2025.



- 1233 ISIMIP terms of use: <https://www.isimip.org/gettingstarted/terms-of-use/>, last access: 28 April 2025.
- 1234 Jägermeyr, J., Müller, C., Ruane, A. C., Elliott, J., Balkovic, J., Castillo, O., Faye, B., Foster, I., Folberth, C.,
1235 Franke, J. A., Fuchs, K., Guarin, J. R., Heinke, J., Hoogenboom, G., Iizumi, T., Jain, A. K., Kelly, D.,
1236 Khabarov, N., Lange, S., ... Rosenzweig, C. (2021). Climate impacts on global agriculture emerge
1237 earlier in new generation of climate and crop models. *Nature Food*, 2(11), 873–885.
1238 <https://doi.org/10.1038/s43016-021-00400-y>
- 1239 John, J. G., Blanton, C., McHugh, C., Radhakrishnan, A., Rand, K., Vahlenkamp, H., Wilson, C., Zadeh, N.,
1240 T., Dunne, J. P., Dussin, R., Horowitz, L. W., Krasting, J. P., Lin, P., Malyshev, S., Naik, V., Ploshay, J.,
1241 Shevliakova, E., Silvers, L., Stock, C., ... Zeng, Y. (2018). *NOAA-GFDL GFDL-ESM4 model output*
1242 *prepared for CMIP6 ScenarioMIP* [Dataset]. Earth System Grid Federation.
1243 <https://doi.org/10.22033/ESGF/CMIP6.1414>
- 1244 Jungclaus, J., Bittner, M., Wieners, K.-H., Wachsman, F., Schupfner, M., Legutke, S., Giorgetta, M., Reick,
1245 C., Gayler, V., Haak, H., de Vrese, P., Raddatz, T., Esch, M., Mauritsen, T., von Storch, J.-S., Behrens,
1246 J., Brovkin, V., Claussen, M., Crueger, T., ... Roeckner, E. (2019). *MPI-M MPIESM1.2-HR model output*
1247 *prepared for CMIP6 CMIP* [Dataset]. Earth System Grid Federation.
1248 <https://doi.org/10.22033/ESGF/CMIP6.741>
- 1249 Kaplan, J. O., Koch, A., & Lau, K. H.-K. (2023). *Estimated future global lightning strokes (2010-2100)*.
1250 <https://doi.org/10.5281/zenodo.7511843>
- 1251 Kaplan, J. O., & Lau, K. H.-K. (2021). The WGLC global gridded lightning climatology and time series.
1252 *Earth System Science Data*, 13(7), 3219–3237. <https://doi.org/10.5194/essd-13-3219-2021>
- 1253 Kaplan, J. O., & Lau, K. H.-K. (2022). World Wide Lightning Location Network (WWLLN) Global Lightning
1254 Climatology (WGLC) and time series, 2022 update. *Earth System Science Data*, 14(12), 5665–5670.
1255 <https://doi.org/10.5194/essd-14-5665-2022>
- 1256 Krasting, J. P., John, J. G., Blanton, C., McHugh, C., Nikonov, S., Radhakrishnan, A., Rand, K., Zadeh, N. T.,



- 1257 Balaji, V., Durachta, J., Dupuis, C., Menzel, R., Robinson, T., Underwood, S., Vahlenkamp, H., Dunne,
1258 K. A., Gauthier, P. P. G., Ginoux, P., Griffies, S. M., ... Zhao, M. (2018). *NOAA-GFDL GFDL-ESM4 model*
1259 *output prepared for CMIP6 CMIP* [Dataset]. Earth System Grid Federation.
1260 <https://doi.org/10.22033/ESGF/CMIP6.1407>
- 1261 Lange, S. (2017). *ISIMIP2b Bias-Correction Code*. <https://doi.org/10.5281/zenodo.1069050>
- 1262 Lange, S. (2018). Bias correction of surface downwelling longwave and shortwave radiation for the
1263 EWEMBI dataset. *Earth System Dynamics*, 9(2), 627–645. <https://doi.org/10.5194/esd-9-627-2018>
- 1264 Lange, S. (2019a). *Earth2Observe, WFDEI and ERA-interim data merged and bias-corrected for ISIMIP*
1265 *(EWEMBI)* [Dataset]. <https://doi.org/10.5880/pik.2019.004>
- 1266 Lange, S. (2019b). Trend-preserving bias adjustment and statistical downscaling with ISIMIP3BASD
1267 (v1.0). *Geoscientific Model Development*, 12(7), 3055–3070.
1268 <https://doi.org/10.5194/gmd-12-3055-2019>
- 1269 Lange, S. (2021a). *ISIMIP3BASD*. <https://doi.org/10.5281/zenodo.4686991>
- 1270 Lange, S. (2021b). *ISIMIP3b bias adjustment fact sheet*.
1271 https://www.isimip.org/documents/413/ISIMIP3b_bias_adjustment_fact_sheet_Gnsz7CO.pdf
- 1272 Lange, S., Menz, C., Gleixner, S., Cucchi, M., Weedon, G. P., Amici, A., Bellouin, N., Schmied, H. M.,
1273 Hersbach, H., Buontempo, C., & Cagnazzo, C. (2021). *WFDE5 over land merged with ERA5 over the*
1274 *ocean (W5E5 v2.0)* [Dataset]. ISIMIP Repository. <https://doi.org/10.48364/ISIMIP.342217>
- 1275 Lange, S., Quesada-Chacón, D., & Büchner, M. (2023). *Secondary ISIMIP3b bias-adjusted atmospheric*
1276 *climate input data* [Dataset]. ISIMIP Repository. <https://doi.org/10.48364/ISIMIP.581124.3>
- 1277 Lan, X., Tans, P., & Thoning, K. W. (2023). *Trends in globally-averaged CO2 determined from NOAA Global*
1278 *Monitoring Laboratory measurements. Version 2023-01 NOAA/GML* [Dataset].
1279 <https://gml.noaa.gov/ccgg/trends/>
- 1280 Large W. G., A. S. G. Y. (2004). *Diurnal to decadal global forcing for ocean and sea ice models: the data*



- 1281 *sets and flux climatologies* (No. NCAR/TN460+STR). CGD Division of the National Centre for
1282 Atmospheric Research (NCAR).
1283 [https://www.researchgate.net/profile/Stephen-Yeager/publication/281588002_Diurnal_to_Decadal](https://www.researchgate.net/profile/Stephen-Yeager/publication/281588002_Diurnal_to_Decadal_Global_Forcing_for_Ocean_and_Sea-Ice_Models_The_Data_Sets_and_Flux_Climatologies/links/55eede7108ae199d47bfaf41/Diurnal-to-Decadal-Global-Forcing-for-Ocean-and-Sea-Ice-Models-The-Data-Sets-and-Flux-Climatologies.pdf)
1284 [l_Global_Forcing_for_Ocean_and_Sea-Ice_Models_The_Data_Sets_and_Flux_Climatologies/links/5](https://www.researchgate.net/profile/Stephen-Yeager/publication/281588002_Diurnal_to_Decadal_Global_Forcing_for_Ocean_and_Sea-Ice_Models_The_Data_Sets_and_Flux_Climatologies/links/55eede7108ae199d47bfaf41/Diurnal-to-Decadal-Global-Forcing-for-Ocean-and-Sea-Ice-Models-The-Data-Sets-and-Flux-Climatologies.pdf)
1285 [5eede7108ae199d47bfaf41/Diurnal-to-Decadal-Global-Forcing-for-Ocean-and-Sea-Ice-Models-The-](https://www.researchgate.net/profile/Stephen-Yeager/publication/281588002_Diurnal_to_Decadal_Global_Forcing_for_Ocean_and_Sea-Ice_Models_The_Data_Sets_and_Flux_Climatologies/links/55eede7108ae199d47bfaf41/Diurnal-to-Decadal-Global-Forcing-for-Ocean-and-Sea-Ice-Models-The-Data-Sets-and-Flux-Climatologies.pdf)
1286 [Data-Sets-and-Flux-Climatologies.pdf](https://www.researchgate.net/profile/Stephen-Yeager/publication/281588002_Diurnal_to_Decadal_Global_Forcing_for_Ocean_and_Sea-Ice_Models_The_Data_Sets_and_Flux_Climatologies/links/55eede7108ae199d47bfaf41/Diurnal-to-Decadal-Global-Forcing-for-Ocean-and-Sea-Ice-Models-The-Data-Sets-and-Flux-Climatologies.pdf)
1287 Lee, C.-Y., Camargo, S. J., Sobel, A. H., & Tippett, M. K. (2020). Statistical–Dynamical Downscaling
1288 Projections of Tropical Cyclone Activity in a Warming Climate: Two Diverging Genesis Scenarios.
1289 *Journal of Climate*, 33(11), 4815–4834. <https://doi.org/10.1175/JCLI-D-19-0452.1>
1290 Lee, C.-Y., Tippett, M. K., Camargo, S. J., & Sobel, A. H. (2015). Probabilistic Multiple Linear Regression
1291 Modeling for Tropical Cyclone Intensity. *Monthly Weather Review*, 143(3), 933–954.
1292 <https://doi.org/10.1175/MWR-D-14-00171.1>
1293 Lee, C.-Y., Tippett, M. K., Sobel, A. H., & Camargo, S. J. (2016). Rapid intensification and the bimodal
1294 distribution of tropical cyclone intensity. *Nature Communications*, 7, 10625.
1295 <https://doi.org/10.1038/ncomms10625>
1296 Lee, C.-Y., Tippett, M. K., Sobel, A. H., & Camargo, S. J. (2018). An environmentally forced tropical cyclone
1297 hazard model. *Journal of Advances in Modeling Earth Systems*, 10(1), 223–241.
1298 <https://doi.org/10.1002/2017ms001186>
1299 Lengaigne, M., Pang, S., Silvy, Y., Danielli, V., Gopika, S., Sadhvi, K., Dutheil, C., Rousset, C., Ethé, C.,
1300 Person, R., Madec, G., Barrier, N., Maury, O., Dalaut, L., Menkes, C., Nicol, S., Gorgues, T., Melet, A.,
1301 & Guihou, K. (2025). Vialard: An ocean modelling framework for mitigating oceanic projections
1302 from global climate models present-day biases. In *Earth future*.
1303 Li, G., Xie, S.-P., Du, Y., & Luo, Y. (2016). Effects of excessive equatorial cold tongue bias on the
1304 projections of tropical Pacific climate change. Part I: the warming pattern in CMIP5 multi-model



- 1305 ensemble. *Climate Dynamics*, 47(12), 3817–3831. <https://doi.org/10.1007/s00382-016-3043-5>
- 1306 Madec, G. (2015). NEMO ocean engine, Version 3.6 stable Note du Pole de modelisation de l'Institut
- 1307 Pierre-Simon Laplace, vol. 27. *IPSL, Paris: France*.
- 1308 Maraun, D. (2013). Bias Correction, Quantile Mapping, and Downscaling: Revisiting the Inflation Issue.
- 1309 *Journal of Climate*, 26(6), 2137–2143. <https://doi.org/10.1175/JCLI-D-12-00821.1>
- 1310 Mauritsen, T., Bader, J., Becker, T., Behrens, J., Bittner, M., Brokopf, R., Brovkin, V., Claussen, M., Crueger,
- 1311 T., Esch, M., Fast, I., Fiedler, S., Fläschner, D., Gayler, V., Giorgetta, M., Goll, D. S., Haak, H.,
- 1312 Hagemann, S., Hedemann, C., ... Roeckner, E. (2019). Developments in the MPI-M Earth System
- 1313 Model version 1.2 (MPI-ESM1.2) and Its Response to Increasing CO₂. *Journal of Advances in*
- 1314 *Modeling Earth Systems*, 11(4), 998–1038. <https://doi.org/10.1029/2018MS001400>
- 1315 Meehl, G. A., Senior, C. A., Eyring, V., Flato, G., Lamarque, J.-F., Stouffer, R. J., Taylor, K. E., & Schlund, M.
- 1316 (2020). Context for interpreting equilibrium climate sensitivity and transient climate response from
- 1317 the CMIP6 Earth system models. *Science Advances*, 6(26), eaba1981.
- 1318 <https://doi.org/10.1126/sciadv.aba1981>
- 1319 Meiler, S., Vogt, T., Bloemendaal, N., Ciullo, A., Lee, C.-Y., Camargo, S. J., Emanuel, K., & Bresch, D. N.
- 1320 (2022). Intercomparison of regional loss estimates from global synthetic tropical cyclone models.
- 1321 *Nature Communications*, 13(1), 6156. <https://doi.org/10.1038/s41467-022-33918-1>
- 1322 Meinshausen, M., Nicholls, Z. R. J., Lewis, J., Gidden, M. J., Vogel, E., Freund, M., Beyerle, U., Gessner, C.,
- 1323 Nauels, A., Bauer, N., Canadell, J. G., Daniel, J. S., John, A., Krummel, P. B., Luderer, G.,
- 1324 Meinshausen, N., Montzka, S. A., Rayner, P. J., Reimann, S., ... Wang, R. H. J. (2020). The shared
- 1325 socio-economic pathway (SSP) greenhouse gas concentrations and their extensions to 2500.
- 1326 *Geoscientific Model Development*, 13(8), 3571–3605. <https://doi.org/10.5194/gmd-13-3571-2020>
- 1327 Meinshausen, M., Smith, S. J., Calvin, K., Daniel, J. S., Kainuma, M. L. T., Lamarque, J.-F., Matsumoto, K.,
- 1328 Montzka, S. A., Raper, S. C. B., Riahi, K., Thomson, A., Velders, G. J. M., & van Vuuren, D. P. P. (2011).



- 1329 The RCP greenhouse gas concentrations and their extensions from 1765 to 2300. *Climatic Change*,
1330 109(1), 213. <https://doi.org/10.1007/s10584-011-0156-z>
- 1331 Meinshausen, M., Vogel, E., Nauels, A., Lorbacher, K., Meinshausen, N., Etheridge, D. M., Fraser, P. J.,
1332 Montzka, S. A., Rayner, P. J., Trudinger, C. M., Krummel, P. B., Beyerle, U., Canadell, J. G., Daniel, J.
1333 S., Enting, I. G., Law, R. M., Lunder, C. R., O'Doherty, S., Prinn, R. G., ... Weiss, R. (2017). Historical
1334 greenhouse gas concentrations for climate modelling (CMIP6). *Geoscientific Model Development*,
1335 10(5), 2057–2116. <https://doi.org/10.5194/gmd-10-2057-2017>
- 1336 Muis, S., Aerts, J. C. J. H., Á. Antolínez, J. A., Dullaart, J. C., Duong, T. M., Erikson, L., Haarsma, R. J.,
1337 Apecechea, M. I., Mengel, M., Le Bars, D., O'Neill, A., Ranasinghe, R., Roberts, M. J., Verlaan, M.,
1338 Ward, P. J., & Yan, K. (2023). Global projections of storm surges using high-resolution CMIP6 climate
1339 models. *Earth's Future*, 11(9). <https://doi.org/10.1029/2023ef003479>
- 1340 Muis, S., Apecechea, M. I., Dullaart, J., de Lima Rego, J., Madsen, K. S., Su, J., Yan, K., & Verlaan, M.
1341 (2020). A High-Resolution Global Dataset of Extreme Sea Levels, Tides, and Storm Surges, Including
1342 Future Projections. *Frontiers in Marine Science*, 7. <https://doi.org/10.3389/fmars.2020.00263>
- 1343 Perrette, M., & Mengel, M. (submitted 2024). *Relative sea level projections constrained by historical*
1344 *trends at tide gauge sites*.
- 1345 Righi, M., Andela, B., Eyring, V., Lauer, A., Predoi, V., Schlund, M., Vegas-Regidor, J., Bock, L., Brötz, B., de
1346 Mora, L., Diblen, F., Dreyer, L., Drost, N., Earnshaw, P., Hassler, B., Koldunov, N., Little, B., Loosveldt
1347 Tomas, S., & Zimmermann, K. (2020). Earth System Model Evaluation Tool (ESMValTool) v2.0 –
1348 technical overview. *Geoscientific Model Development*, 13(3), 1179–1199.
1349 <https://doi.org/10.5194/gmd-13-1179-2020>
- 1350 Ruosteenoja, K., Jylhä, K., Räisänen, J., & Mäkelä, A. (2017). Surface air relative humidities spuriously
1351 exceeding 100% in CMIP5 model output and their impact on future projections. *JGR Atmospheres*,
1352 122(18), 9557–9568. <https://doi.org/10.1002/2017JD026909>



- 1353 Ruosteenoja, K., Jylhä, K., Räisänen, J., & Mäkelä, A. (2018). Reply to comment by genthon et al. On
1354 “surface air relative humidities spuriously exceeding 100% in CMIP5 model output and their impact
1355 on future projections.” *Journal of Geophysical Research*, 123(16), 8728–8734.
1356 <https://doi.org/10.1029/2018jd028680>
- 1357 Schupfner, M., Wieners, K.-H., Wachsmann, F., Steger, C., Bittner, M., Jungclaus, J., Früh, B., Pankatz, K.,
1358 Giorgetta, M., Reick, C., Legutke, S., Esch, M., Gayler, V., Haak, H., de Vrese, P., Raddatz, T.,
1359 Mauritsen, T., von Storch, J.-S., Behrens, J., ... Roeckner, E. (2019). *DKRZ MPI-ESM1.2-HR model*
1360 *output prepared for CMIP6 ScenarioMIP* [Dataset]. Earth System Grid Federation.
1361 <https://doi.org/10.22033/ESGF/CMIP6.2450>
- 1362 Séférian, R., Berthet, S., Yool, A., Palmiéri, J., Bopp, L., Tagliabue, A., Kwiatkowski, L., Aumont, O.,
1363 Christian, J., Dunne, J., Gehlen, M., Ilyina, T., John, J. G., Li, H., Long, M. C., Luo, J. Y., Nakano, H.,
1364 Romanou, A., Schwinger, J., ... Yamamoto, A. (2020). Tracking Improvement in Simulated Marine
1365 Biogeochemistry Between CMIP5 and CMIP6. *Current Climate Change Reports*, 6(3), 95–119.
1366 <https://doi.org/10.1007/s40641-020-00160-0>
- 1367 Sellar, A. A., Jones, C. G., Mulcahy, J. P., Tang, Y., Yool, A., Wiltshire, A., O’Connor, F. M., Stringer, M., Hill,
1368 R., Palmieri, J., Woodward, S., Mora, L., Kuhlbrodt, T., Rumbold, S. T., Kelley, D. I., Ellis, R., Johnson,
1369 C. E., Walton, J., Abraham, N. L., ... Zerroukat, M. (2019). UKESM1: Description and evaluation of
1370 the U.k. earth system model. *Journal of Advances in Modeling Earth Systems*, 11(12), 4513–4558.
1371 <https://doi.org/10.1029/2019ms001739>
- 1372 Shiogama, H., Fujimori, S., Hasegawa, T., Hayashi, M., Hirabayashi, Y., Ogura, T., Iizumi, T., Takahashi, K.,
1373 & Takemura, T. (2023). Important distinctiveness of SSP3–7.0 for use in impact assessments. *Nature*
1374 *Climate Change*, 13(12), 1276–1278. <https://doi.org/10.1038/s41558-023-01883-2>
- 1375 Sobel, A. H., Lee, C.-Y., Bowen, S. G., Camargo, S. J., Cane, M. A., Clement, A., Fosu, B., Hart, M., Reed, K.
1376 A., Seager, R., & Tippett, M. K. (2021). Near-term tropical cyclone risk and coupled Earth system



- 1377 model biases. *Proceedings of the National Academy of Sciences of the United States of America* ,
1378 120(33), e2209631120. <https://doi.org/10.1073/pnas.2209631120>
- 1379 Sobel, A. H., Lee, C.-Y., Camargo, S. J., Mandli, K. T., Emanuel, K. A., Mukhopadhyay, P., & Mahakur, M.
1380 (2019). Tropical Cyclone Hazard to Mumbai in the Recent Historical Climate. *Monthly Weather*
1381 *Review*, 147(7), 2355–2366. <https://doi.org/10.1175/MWR-D-18-0419.1>
- 1382 Stewart, K. D., Kim, W. M., Urakawa, S., Hogg, A. M., Yeager, S., Tsujino, H., Nakano, H., Kiss, A. E., &
1383 Danabasoglu, G. (2020). JRA55-do-based repeat year forcing datasets for driving ocean–sea-ice
1384 models. *Ocean Modelling*, 147, 101557. <https://doi.org/10.1016/j.ocemod.2019.101557>
- 1385 Switanek, M. B., Troch, P. A., Castro, C. L., Leuprecht, A., Chang, H.-I., Mukherjee, R., & Demaria, E. M. C.
1386 (2017). Scaled distribution mapping: a bias correction method that preserves raw climate model
1387 projected changes. *Hydrology and Earth System Sciences*, 21(6), 2649–2666.
1388 <https://doi.org/10.5194/hess-21-2649-2017>
- 1389 Tagliabue, A., Kwiatkowski, L., Bopp, L., Butenschön, M., Cheung, W., Lengaigne, M., & Vialard, J. (2021).
1390 Persistent Uncertainties in Ocean Net Primary Production Climate Change Projections at Regional
1391 Scales Raise Challenges for Assessing Impacts on Ecosystem Services. *Frontiers in Climate*, 3.
1392 <https://doi.org/10.3389/fclim.2021.738224>
- 1393 Tang, Y., Rumbold, S., Ellis, R., Kelley, D., Mulcahy, J., Sellar, A., Walton, J., & Jones, C. (2019). *MOHC*
1394 *UKESM1.0-LL model output prepared for CMIP6 CMIP* [Dataset]. Earth System Grid Federation.
1395 <https://doi.org/10.22033/ESGF/CMIP6.1569>
- 1396 Themeßl, M. J., Gobiet, A., & Heinrich, G. (2012). Empirical-statistical downscaling and error correction
1397 of regional climate models and its impact on the climate change signal. *Climatic Change*, 112(2),
1398 449–468. <https://doi.org/10.1007/s10584-011-0224-4>
- 1399 Thrasher, B., Maurer, E. P., McKellar, C., & Duffy, P. B. (2012). Technical Note: Bias correcting climate
1400 model simulated daily temperature extremes with quantile mapping. *Hydrology and Earth System*



- 1401 *Sciences*, 16(9), 3309–3314. <https://doi.org/10.5194/hess-16-3309-2012>
- 1402 Tippett, M. K., Camargo, S. J., & Sobel, A. H. (2011). A Poisson Regression Index for Tropical Cyclone
- 1403 Genesis and the Role of Large-Scale Vorticity in Genesis. *Journal of Climate*, 24(9), 2335–2357.
- 1404 <https://doi.org/10.1175/2010JCLI3811.1>
- 1405 Treu, S., Muis, S., Dangendorf, S., Wahl, T., Oelsmann, J., Heinicke, S., Frieler, K., & Mengel, M. (2023).
- 1406 Reconstruction of hourly coastal water levels and counterfactuals without sea level rise for impact
- 1407 attribution. In *Earth System Science Data Discussions*. <https://doi.org/10.5194/essd-2023-112>
- 1408 Tsujino, H., Urakawa, L. S., Griffies, S. M., Danabasoglu, G., Adcroft, A. J., Amaral, A. E., Arsouze, T.,
- 1409 Bentsen, M., Bernardello, R., Böning, C. W., Bozec, A., Chassignet, E. P., Danilov, S., Dussin, R.,
- 1410 Exarchou, E., Fogli, P. G., Fox-Kemper, B., Guo, C., Ilıcak, M., ... Yu, Z. (2020). Evaluation of global
- 1411 ocean–sea-ice model simulations based on the experimental protocols of the Ocean Model
- 1412 Intercomparison Project phase 2 (OMIP-2). *Geoscientific Model Development*, 13(8), 3643–3708.
- 1413 <https://doi.org/10.5194/gmd-13-3643-2020>
- 1414 Weedon, G. P., Gomes, S., Viterbo, P., Österle, H., Adam, J. C., Bellouin, N., Boucher, O., & Best, M.
- 1415 (2010). *The watch forcing data 1958-2001: a meteorological forcing data set for land surface- and*
- 1416 *hydrological-models*. 41. https://publications.pik-potsdam.de/pubman/item/item_16400
- 1417 Woodworth-Jefcoats, P. (2022). *therMizer-FishMIP-2022-HI: Code and data for FishMIP 2022 ISIMIP 3a -*
- 1418 *Hawaii longline fishing ground regional model*. Github.
- 1419 <https://github.com/pwoodworth-jefcoats/therMizer-FishMIP-2022-HI>
- 1420 Yukimoto, S., Kawai, H., Koshiro, T., Oshima, N., Yoshida, K., Urakawa, S., Tsujino, H., Deushi, M., Tanaka,
- 1421 T., Hosaka, M., Yabu, S., Yoshimura, H., Shindo, E., Mizuta, R., Obata, A., Adachi, Y., & Ishii, M.
- 1422 (2019). The Meteorological Research Institute Earth System Model Version 2.0, MRI-ESM2.0:
- 1423 Description and Basic Evaluation of the Physical Component. *Journal of the Meteorological Society*
- 1424 *of Japan. Ser. II*, 97(5), 931–965. <https://doi.org/10.2151/jmsj.2019-051>



- 1425 Yukimoto, S., Koshiro, T., Kawai, H., Oshima, N., Yoshida, K., Urakawa, S., Tsujino, H., Deushi, M., Tanaka,
1426 T., Hosaka, M., Yoshimura, H., Shindo, E., Mizuta, R., Ishii, M., Obata, A., & Adachi, Y. (2019a). *MRI*
1427 *MRI-ESM2.0 model output prepared for CMIP6 CMIP* [Dataset]. Earth System Grid Federation.
1428 <https://doi.org/10.22033/ESGF/CMIP6.621>
- 1429 Yukimoto, S., Koshiro, T., Kawai, H., Oshima, N., Yoshida, K., Urakawa, S., Tsujino, H., Deushi, M., Tanaka,
1430 T., Hosaka, M., Yoshimura, H., Shindo, E., Mizuta, R., Ishii, M., Obata, A., & Adachi, Y. (2019b). *MRI*
1431 *MRI-ESM2.0 model output prepared for CMIP6 ScenarioMIP* [Dataset]. Earth System Grid
1432 Federation. <https://doi.org/10.22033/ESGF/CMIP6.638>
- 1433 Zhu, L., Quiring, S. M., & Emanuel, K. A. (2013). Estimating tropical cyclone precipitation risk in Texas.
1434 *Geophysical Research Letters*, 40(23), 6225–6230. <https://doi.org/10.1002/2013gl058284>